

Lightweight Model Attribution and Detection of Synthetic Speech via Audio Residual Fingerprints

Matías Pizarro¹ Mike Laszkiewicz¹ Dorothea Kolossa² Asja Fischer¹

¹Faculty of Computer Science, Ruhr University Bochum, Germany

²Electronic Systems of Medical Engineering, Technische Universität Berlin, Germany

Abstract—As speech generation technologies advance, so do risks of impersonation, misinformation, and spoofing. We present a lightweight, training-free approach for detecting synthetic speech and attributing it to its source model. Our method addresses three tasks: (1) single-model attribution in an open-world setting, (2) multi-model attribution in a closed-world setting, and (3) real vs. synthetic speech classification. The core idea is simple: we compute standardized average residuals—the difference between an audio signal and its filtered version—to extract model-agnostic fingerprints that capture synthesis artifacts. Experiments across multiple synthesis systems and languages show AUROC scores above 99%, with strong reliability even when only a subset of model outputs is available. The method maintains high performance under common audio distortions, including echo and moderate background noise, while data augmentation can improve results in more challenging conditions. In addition, out-of-domain detection is performed using Mahalanobis distances to in-domain residual fingerprints, achieving an F1 score of 0.91 on unseen models, reinforcing the method’s efficiency, generalizability, and suitability for digital forensics and security applications.

Index Terms—synthetic speech classification, model attribution, digital forensics, residual fingerprints.

I. INTRODUCTION

With the rapid advancement of synthetic data generation technologies, distinguishing between genuine and artificial speech signals has become increasingly challenging. Public and open-source tools now enable even unskilled attackers to synthesize highly realistic voice samples that closely resemble human speech [1], [2]. While these technologies offer clear benefits, such as improving availability for speech-impaired individuals [3] and supporting multilingual communication [4], they also pose several security risks. Spoofing attacks on Automatic Speaker Verification (ASV) systems, impersonation of trusted speakers, and misuse in voice-controlled interfaces are all well-documented threats. These threats can be exploited in various harmful ways, such as disinformation campaigns [5], bypassing biometric authentication [6], forging audio evidence in legal contexts [7], or conducting identity fraud through voice cloning [8], [9]. The emergence of synthetic audio as a vector for impersonation and manipulation presents a direct challenge to the security and trustworthiness of modern communication systems. Current defenses largely focus on binary deepfake detection, i.e., deciding whether an audio signal is real or synthetic. While this line of research is valuable and reflected in benchmark challenges such as Automatic Speaker

Verification Spoofing (ASVspoof) [10] and Audio Deepfake Detection (ADD) [11], it addresses only part of the problem. Detection confirms manipulation, but attribution identifies the system responsible for the forgery. This distinction is critical across forensic, legal, and security domains.

Attribution matters for two reasons. First, it provides actionable threat intelligence: linking an attack to a particular synthesis model reveals whether adversaries relied on commercial APIs, open-source implementations, or proprietary tools, thereby informing risk assessment, replication potential, and mitigation strategies. Second, it underpins accountability and legal claims: rights holders can identify misuse of proprietary models, and prosecutors can strengthen evidence chains by showing not just that an audio sample is fake, but also how it was generated. The consequences of lacking attribution are evident in real-world incidents, e.g., in June 2025, adversaries used AI voice cloning to impersonate U.S. Secretary of State Marco Rubio, contacting foreign ministers via Signal and voicemail in an operation designed to extract sensitive information [12]. While detection alone could flag the audio as fake, attribution would have offered critical intelligence about the tool employed, accelerating response and mitigation. Compared to detection, *model attribution* (or *algorithm recognition*) is still relatively underexplored, particularly in the context of audio. Despite the risk of misattribution, simple and efficient methods can still offer meaningful insights for forensic and security purposes. Our work takes a step in this direction by showing how lightweight attribution can be both feasible and effective.

Recent studies have explored multiclass classification approaches to attribute speech samples to specific synthesis systems. However, these models operate in a closed-world setting [13], [14], which means that they can only recognize systems seen during training. As a result, they do not generalize to new models without costly retraining, which presents a major limitation given the rapid evolution of synthetic speech technologies. To address these challenges, we propose a novel, lightweight, training-free approach, referred to as the *Residual Fingerprint (RFP)*. The RFP is computed from standardized average residuals of the audio signal and can be used for both speech synthesis system attribution and synthetic speech classification. To the best of our knowledge, we introduce the first single-model attribution technique in an open-world setting, i.e., a technique for identifying whether a speech

sample was generated by a specific model while distinguishing it from any unseen speech synthesis systems or even from real speech. Notably, our method only requires samples from *one* target model and does not require training a costly machine learning classifier, making it highly adaptable to emerging speech synthesis technologies. Moreover, it naturally extends to closed-world multi-model attribution and synthetic vs. real speech classification, providing a unified solution across multiple threat scenarios. Experiments show that it outperforms existing baselines while remaining efficient, easy to deploy, and robust to realistic noise, with data augmentation helping maintain performance under more severe corruptions. Building on these insights, our key contributions are:

- **Discovery of model-specific speech residual fingerprints:** Speech synthesis systems leave subtle but consistent artifacts in generated audio. These residual patterns serve as reliable, model-specific fingerprints across diverse samples.
- **A unified, lightweight, training-free framework:** Leveraging these residual fingerprints, the method performs single- and multi-model attribution as well as synthetic vs. real classification, requiring only samples from the target model and no costly classifier training.
- **Extensive empirical validation:** Evaluated on a broad range of synthetic audio—including neural vocoders, neural codec-based systems, and other modern synthesis models—across multiple languages and generation approaches, achieving excellent results in both open- and closed-world scenarios.
- **Robustness evaluation:** Demonstrates resilience to moderate background noise, with data augmentation helping maintain performance under more severe audio corruptions, highlighting suitability for practical forensic and security applications.

By addressing both attribution and classification of synthetic speech, this work advances lightweight, deployable defenses against malicious uses of generative models, contributing directly to applied cybersecurity and digital forensics.

II. PROBLEM SETUP AND THREAT MODELS

The rise of advanced speech synthesis models—including text-to-speech (TTS) [15], voice conversion (VC) [16], and neural codec-based generators [17]—poses a significant threat to the integrity and trustworthiness of modern communication systems. TTS systems generate speech from arbitrary text inputs using a target speaker’s voice, while VC systems modify a source speaker’s voice to resemble a target speaker’s voice, preserving the linguistic content. Neural codec-based generators can produce synthetic audio by compressing and reconstructing speech, potentially combining characteristics of both TTS and VC, or performing other generative transformations. From a security and forensics perspective, it is critical to develop techniques that can reliably detect AI-generated audio. However, detection alone is not sufficient: it is equally important to attribute synthetic speech to its generative source. Attribution enables defenders to (1) trace

the origin of misinformation or impersonation attacks, (2) hold the creators of malicious content accountable, and (3) design targeted countermeasures against specific synthesis models. For instance, in high-security environments such as banking voice authentication or governmental communications, systems might deploy lightweight model-specific classifiers to flag suspicious audio in real time, apply adaptive thresholds based on the known behavior of the synthesis model, or use model outputs to adversarially train more robust detection systems. Attribution is also important from the perspective of model owners, since it can help detect model theft or the illegal use of a model.

Attacker model: We assume a non-adaptive adversary with access to one or more generative speech models. These may be public (e.g., open-source) or proprietary systems, and the attacker can generate synthetic audio, which is then transmitted to the target system. During transmission, the audio may be subject to lossy transformations such as echo effects, environmental noise, MP3 compression, or reverberation. The adversary does not know which detection or attribution mechanism will be used by the defender.

Defender model: The defender aims to detect or attribute potentially fake audio samples. Their capabilities vary across scenarios—ranging from having access to generated data from only one synthesis model to having data from multiple generators. Attribution relies on the audio samples alone, without knowledge of the internal workings of the generative models.

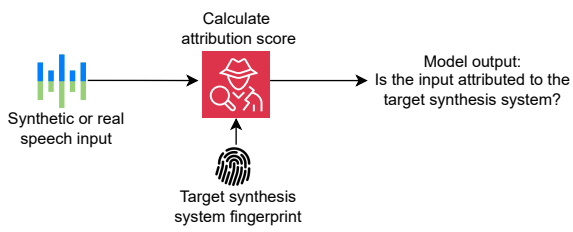
A. Problem Settings

We define the attribution problem along two dimensions:

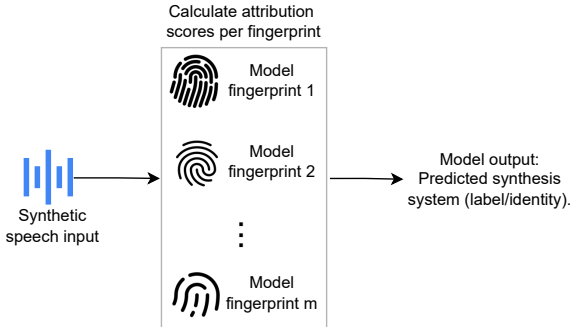
- Single-model vs. multi-model: Data of how many synthesis models is available to the defender for constructing the attribution technique?
- Open-world vs. closed-world: Is the synthesis model used by the attacker assumed to be included in the construction phase of the attribution method, or can it be a previously unseen (unknown) model?

These axes define three core scenarios illustrated in Fig. 1 and detailed below.

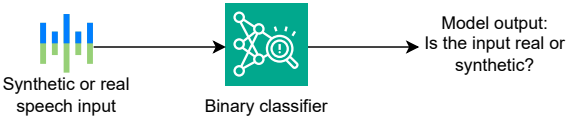
1) *Single-Model Attribution in an Open-World Setting* (Fig. 1a): In this scenario, the defender has training data from only one known synthesis model and aims to determine whether a given audio sample—potentially real, or generated by an unknown system—was synthesized by this specific model. This setting is especially relevant when a particular model is repeatedly used in impersonation attacks or malicious content generation, and the defender needs to determine whether new samples can be attributed to that same source. It represents a challenging and underexplored problem [13], [14], since it requires generalization to unseen distributions of synthetic and natural speech. These distributions may involve (i) different languages, to account for cross-lingual impersonation attempts, (ii) new speakers, to cover emerging targets of attack, and (iii) a variety of advanced synthesis paradigms (e.g., TTS, VC, or neural codec-based generators), which continually broaden the landscape of potential threats.



(a) Single-Model Attribution in an Open-World Setting: Detects whether an audio sample, which could be synthetic or real, has been generated by a specific target speech synthesis system.



(b) Multi-Model Attribution in a Closed-World Setting: Classifies the synthetic audio as originating from one of several known models.



(c) Real vs. Synthetic Classification: Classifies whether the input is genuine human speech or synthetic.

Fig. 1. Architecture of our audio fingerprinting system designed for synthetic audio classification and attribution in operational security contexts. The system ingests audio input and routes it through three complementary modules, each serving a distinct purpose: (a) single-model attribution in an open-world setting, (b) multi-model attribution in a closed-world setting, and (c) real vs. synthetic classification. These components may be deployed independently or in sequence, depending on the application, such as forensic voice analysis, authentication integrity checks, or deepfake detection at content platforms.

2) Multi-Model Attribution in a Closed-World Setting (Fig. 1b): Here, the defender has access to samples from several synthesis models when constructing the attribution technique, and all models encountered at test time are among those known. The goal is to correctly classify which model generated the synthetic input. This closed-world setting has been widely studied in prior work [13], [14], [18], [19], and related studies have also explored the concept of attacker-specific signatures in audio deepfakes [20]. Applications include forensic tracing, where the defender wants to narrow down the toolchain used by an attacker among a known set of synthesis technologies.

3) Real vs. Synthetic classification (Fig. 1c): This classic problem—distinguishing real from generated audio—is well studied in the ASVspoof challenge [10] and typically framed in a multi-model, closed-world setting. Importantly, detection differs from attribution: the challenge separates bona fide vs. spoof discrimination from speaker verification under spoof-

ing attacks, highlighting the need to clearly delineate these tasks.

B. Threat Scenarios in Practice

Each setting corresponds to practical applications with varying levels of difficulty and generalization requirements:

(a) Single-Model Attribution in an Open-World Setting: Critical for model owners, IP protection, and threat monitoring of specific high-risk tools—despite the limited training data.

(b) Multi-Model Attribution in a Closed-World Setting: Useful for law enforcement or forensic analysts who can obtain samples from all suspected models.

(c) Real vs. Synthetic Classification: Widely used in spoofing detection and authentication systems.

III. RELATED WORK

This section reviews existing research on the classification and attribution of synthetic audio—commonly known as audio deepfake detection—focusing on approaches suitable for practical, automated identification of generative model outputs. It also revisits the concept of generative model fingerprints, originally proposed in the computer vision domain for generative adversarial networks (GANs).

A. Deepfake Detection Approaches

Research in deepfake detection spans anti-spoofing techniques and synthesis system attribution methods.

1) Spoofing Detection Systems: These systems typically consist of an acoustic feature extractor and a classifier. The acoustic feature extractor is designed to extract relevant characteristics from the raw audio input, which are then forwarded to the classifier. Examples of spectral features include Linear-Frequency Cepstral Coefficients (LFCC) [21], Mel-Frequency Cepstral Coefficients (MFCC) [21], Constant Q Cepstral Coefficients [22], and long-term variable Q transform [23]. The classifier is then trained on these acoustic features to distinguish real from synthetic audio samples. Classifier models that have demonstrated effectiveness for this task are based on Gaussian mixture models [24] or various types of neural networks like X-vector [25], Light Convolutional Neural Networks (LCNNs) [26], [27], Residual Networks (ResNets) [28]–[30], Squeeze-Excitation and Residual Networks (SE-ResNets) [31]–[33], Graph Attention Networks [34], [35], Differentiable Architecture Search [36], and Transformers [37].

2) Synthesis System Attribution Methods: In contrast, model attribution aims to identify the specific generative synthesis system responsible for producing synthetic audio. Deep learning-based synthesis systems outperform traditional parametric and concatenative methods, generating high-fidelity speech with improved prosody and speaker similarity. Among the leading approaches are GAN-based models [18], which leverage adversarial training to generate high-quality, low-latency speech; Flow-based models [38], which employ invertible transformations for efficient waveform synthesis; Diffusion-based models [39], which refine noise into speech

through iterative processes, achieving state-of-the-art quality at higher computational cost; Hybrid signal processing–deep learning models [40], which combine traditional signal processing techniques with neural networks for greater interpretability; and neural codec-based models [17], which compress and reconstruct audio through learned latent representations, enabling high-quality synthesis that can exhibit characteristics of both TTS and VC systems. These different generative models have been studied in various detection and attribution works, including a subset of studies that explore model fingerprinting. For example, Frank and Schönherr [18] observed that speech generated by GAN-based synthesis systems exhibits high-frequency artifacts. Yan et al. [13] utilized LFCC features and a ResNet classifier to detect audio produced by eight different synthetic speech models, while Li et al. [19] applied MFCCs and a lightweight CNN to classify samples generated by four GAN-based systems. Similarly, Deng et al. [14] employed Mel spectrograms and trained a neural network using contrastive learning to identify synthetic speech generated by six distinct models. Müller et al. [20] introduced attacker signatures via neural embeddings, achieving high accuracy across 4 and 20 known classes. Stan et al. [41] showed that features extracted from the early layers of a pretrained self-supervised model can be used with a k-Nearest Neighbors (kNN) classifier to perform model attribution of generated audio across multiple datasets. However, all the above systems rely on supervised classifiers with fixed label sets, making them inherently closed-set and requiring retraining whenever a new model appears. Our method avoids this limitation entirely by using training-free residual fingerprints that naturally support open-world attribution. Separately, approaches like proactive audio perturbations [42], [43] and digital watermarking [44], [45] fall into different research domain. The former aims to prevent unauthorized synthesis before it occurs, while the latter embeds model-specific information into generated content to enable ownership verification. While effective for privacy and prevention, they are outside the scope of this work; here, we focus on post-hoc model attribution, which complements these strategies by enabling forensic and investigative capabilities.

B. Limitations of Prior Work

Prior efforts, while effective in closed-world settings, struggle with generalization to unknown generative models, often due to overfitting or limited training diversity. Existing audio and image fingerprinting methods either train supervised classifiers tied to specific models (GAN-based synthesizers only) [46], [47], or require paired real–synthetic samples [48], limiting applicability. An example of recent work addressing the open-world scenario is the third track of the ADD 2023 challenge [11]. However, it differs from our approach in three key ways. First, the attribution techniques were evaluated based on data from 8 different sources, of which 7 were known during training. The existence of multiple models during training allows leveraging latent representations of a trained

classifier, as deployed by the winner of the challenge [49], or to make use of contrastive learning, as deployed by the runner-up [50]. In the single-model setting, that is, when restricting access to data from only a single source during training, these techniques are not applicable. Secondly, the evaluation in ADD puts more emphasis on the closed-world performance as the dataset contains around $7/8 = 87.5\%$ samples from generative models seen during training. Lastly, the dataset utilized in ADD is not publicly available, which limits its reproducibility significantly.¹ Separately, most prior works do not evaluate whether their approaches generalize across varying audio corruptions (e.g., environmental noise, compression, reverberation) or on synthetic audio generated by non-GAN-based models. In contrast, our work provides a unified, model-agnostic, lightweight, and training-free framework that extracts inherent residual fingerprints from synthetic audio without the need for paired data, model-specific retraining, or architectural assumptions. This makes it naturally suited for open-world attribution while still supporting closed-world scenarios relevant to practical cybersecurity applications such as fake audio detection and model-source attribution.

C. Revisiting GAN Fingerprints

The concept of model-specific fingerprints was initially explored by Marra et al. [51] in the context of image generation using GANs. Their idea is based on the assumption that any artificially generated image x decomposes into its content $I(x)$ and a fingerprint F that is unrelated to the image semantics but specific to the model, that is, $x = I(x) + F$ for every x generated from the model. To extract the fingerprint, they assumed that a suitable image filter f is capable of removing the fingerprint, such that $f(x) \approx I(x)$, and therefore $R := x - f(x) \approx F$. Given a set of generated samples x_1, \dots, x_N , the sample-wise residuals are defined by $R_i := x_i - f(x_i)$ and F is estimated by $\hat{F} := \frac{1}{N} \sum_{i=1}^N R_i$. For inference, i.e., for checking whether a test sample x_{test} contains a fingerprint similar to \hat{F} , they first compute its residual R_{test} as above and then assign the correlation score $s_{\text{cor}}(x_{\text{test}}; \hat{F}) := \langle \hat{R}_{\text{test}}, \hat{F} \rangle \in [-1, 1]$, where \hat{R}_{test} and \hat{F} denote the zero-mean and unit-norm versions of R_{test} and \hat{F} , respectively. Having a set of m different generative models, and therefore, a set of corresponding fingerprints $\hat{F}_1, \dots, \hat{F}_m$, one attributes a sample to the j th model, where $j = \arg \max_{i \in [m]} s_{\text{cor}}(x_{\text{test}}; \hat{F}_i)$.

IV. METHODOLOGY

Prior fingerprinting methods, such as the residual-based approach of Marra et al. [51], assume that GANs introduce a stable, model-specific artifact that can be isolated by spatial filtering. While effective for early image GANs, later studies—including Ning et al. [46]—show that this method becomes substantially weaker and less reliable for modern architectures. More importantly, these approaches are image-specific and do not account for the temporal variability,

¹The dataset cannot be reproduced because the source of the unknown class is not shared.

spectral structure, and semantic entanglement inherent to audio. Our work introduces a conceptually distinct residual fingerprint tailored to synthetic speech: a training-free, model-agnostic representation operating on spectral energy patterns rather than spatial residuals, enabling attribution across diverse audio generation paradigms such as neural codecs, diffusion models, and hybrid neural-signal processing systems. In the audio domain, a synthetic speech waveform can be conceptually decomposed into its semantic content—linguistic message, speaker identity, prosody—and a residual fingerprint introduced by the specific generative model. This residual reflects subtle, model-specific artifacts embedded during synthesis and forms the basis for attribution, a direction that remains largely unexplored for audio compared to images. Audio signals also pose unique challenges for fingerprint extraction, such as high temporal resolution, dynamic spectral patterns, and variability across speakers and languages. Here, it is useful to distinguish between speech—the structured linguistic and prosodic information—and audio—the full signal, including background noise, recording conditions, and synthesis artifacts. Our approach operates on spectral representations of the waveform to isolate residual fingerprints while minimizing the influence of the speech content itself. This task presents three main challenges that distinguish audio fingerprinting from its image counterpart:

- 1) Variable-length: Unlike fixed-size images, audio signals vary in duration, but fingerprint extraction requires a fixed-size representation for consistent analysis.
- 2) Content-preserving filtering: While image fingerprints rely on spatial filtering, audio requires filters that suppress content-related features such as speech semantics and phonetics, while preserving subtle generative model-specific artifacts.
- 3) Distance metric for attribution: Instead of using correlation, we adopt the Mahalanobis distance, which incorporates the covariance of residual features. This yields greater robustness to intra-model variability and improves discrimination among diverse synthesis systems.

Our pipeline addresses these challenges by first converting each audio sample to an average spectral energy representation and then applying suitable filters to extract residuals, which are averaged to form a fingerprint as detailed in the following.

A. Average Energy Representation

To overcome the length variability of the audio signals, we transform each signal into a fixed-size representation that summarizes its spectral content. We apply the Short-Time Fourier Transform (STFT), which converts a time-domain signal into a time-frequency representation known as a spectrogram. We assume that the input signals are already in discrete-time digital format (i.e., sampled waveforms at a fixed sampling rate). First, let $x^{(i)}$ be a discrete-time audio signal of arbitrary length, representing the i -th sample. Since the frequency content of audio signals typically changes over time, applying a single global Fourier transform would only provide an average frequency representation over the entire signal, thereby losing

important temporal information. To capture how the frequency components evolve, we divide the signal into overlapping short-time frames $x^{(i)}(k, t)$, where $k \in \{0, \dots, L-1\}$ is the time index within each frame of length L (i.e., there are L discrete amplitude values per frame), and $t \in \{1, \dots, T^{(i)}\}$ is the frame index, where $T^{(i)}$ is the total number of frames obtained by sliding a window over signal $x^{(i)}$. Frames are often overlapped (e.g., 25% overlap) to improve temporal continuity and reduce artifacts from abrupt frame boundaries. Therefore, the total number of frames $T^{(i)}$ depends on the signal length, the sampling rate, the frame length L , and the hop size (i.e., the number of samples between consecutive frames). Second, to mitigate spectral leakage at frame boundaries, each frame is multiplied by a smooth window function $\omega(k)$, such as a Hann or Hamming window $x_{\omega}^{(i)}(k, t) = x^{(i)}(k, t) \cdot \omega(k)$. This smooths the signal at the boundaries of each frame before applying the Fourier transform. We then apply the Discrete Fourier Transform (DFT) to each windowed frame $X_{\text{DFT}}^{(i)}(f, t) = \sum_{k=0}^{L-1} x_{\omega}^{(i)}(k, t) \cdot e^{-j2\pi kf/L}$, where $f \in \{0, \dots, L-1\}$ is the frequency bin index, and $X_{\text{DFT}}^{(i)}(f, t) \in \mathbb{C}$ is the complex frequency spectrum of frame t . To obtain the spectrogram, we take the magnitude of the complex spectrum $S_X^{(i)}(f, t) = |X_{\text{DFT}}^{(i)}(f, t)|$. The resulting spectrogram $S_X^{(i)} \in \mathbb{R}^{F \times T^{(i)}}$ represents the signal’s energy distribution over time and frequency, where F is the number of unique frequency bins. We apply a logarithmic transformation to map power values to decibels $\mathcal{S}_X^{(i)}(f, t) = 20 \cdot \log_{10}(S_X^{(i)}(f, t))$. To obtain a fixed-size representation independent of audio length, we compute the average energy per frequency bin:

$$E_{x^{(i)}}[f] := \frac{1}{T^{(i)}} \sum_{t=1}^{T^{(i)}} \mathcal{S}_X^{(i)}(f, t),$$

yielding a vector $E_{x^{(i)}} \in \mathbb{R}^F$ that summarizes the spectral energy distribution across time. This time-frequency representation forms the basis for our subsequent fingerprint estimation method that requires a fixed-size input.

B. Suitable Filtering Methods

To isolate generative artifacts, we apply content-preserving filters to the audio signal before computing the residuals of our spectral energy representation. We investigate two types of filtering approaches: neural compression using EnCodec, and Finite Impulse Response (FIR) spectral filtering, including low-pass, high-pass, band-stop, and band-pass filters. The choice of EnCodec and FIR spectral filtering is motivated by prior findings. In the image domain, Yu et al. [46] showed that compression/denoising preserves GAN fingerprints, while in audio, the WaveFake study [18] using paired real–synthetic samples demonstrated that compression and bandwidth reduction retain synthesis artifacts in high-frequency regions. Following this principle, we employ EnCodec and FIR filtering as alternative content-preserving preprocessing methods. EnCodec removes fine speech detail through learned compression, aligning with the findings from the image domain, whereas FIR filtering

provides an interpretable way to attenuate content-dominant frequency regions, consistent with the observations in the audio domain. Both are used independently to expose residual artifacts before fingerprint extraction.

EnCodec [52]: It is a neural audio compression model based on a quantized latent representation. We use a pre-trained causal model operating at 24 kHz on monophonic audio, trained on a variety of audio data.² It consists of an encoder that transforms the input waveform into a latent vector \mathbf{w} , a quantizer that maps \mathbf{w} to a discretized version \mathbf{w}_q , and a decoder that reconstructs the waveform from \mathbf{w}_q . This architecture preserves the overall content while discarding fine-grained details, making it suitable for suppressing speech synthesis-specific artifacts.

Spectral Filtering: As an alternative to neural compression, we apply FIR filtering to manipulate the spectral characteristics of the audio signal in a controlled and interpretable manner. By selectively preserving or attenuating different frequency bands—such as low, high, or mid frequencies—we aim to suppress content-related information while retaining generative artifacts introduced by the synthesis model. An FIR filter operates by convolving the input signal with a set of learned or designed filter coefficients. Given a discrete-time input signal $x^{(i)} = \{x_1^{(i)}, x_2^{(i)}, \dots, x_s^{(i)}\}$, the filtered output $y^{(i)} = \{y_1^{(i)}, y_2^{(i)}, \dots, y_s^{(i)}\}$ is obtained via convolution: $y_n^{(i)} = \sum_{k=0}^{K-1} h_k \cdot x_{n-k}^{(i)}$, for $n = 1, \dots, s$, where h_k are the filter coefficients, and K is the filter order, i.e., the number of coefficients in the FIR filter. Zero-padding is applied when $n - k < 1$. This corresponds to a standard 1D convolution operation with one input and one output channel. By choosing appropriate coefficients, we can implement low-pass, high-pass, band-stop, or band-pass behavior depending on which frequency bands we aim to isolate or suppress.

C. Residual Fingerprint Extraction

Given a set of N audio signals $\{x^{(i)}\}_{i=1}^N$, we estimate the generative model’s fingerprint $\hat{\mathcal{F}}$ by averaging the residuals between the original and filtered average energy representations:

$$\hat{\mathcal{F}} := \frac{1}{N} \sum_{i=1}^N \mathcal{R}^{(i)}, \text{ where } \mathcal{R}^{(i)} := E_{x^{(i)}} - E_{f(x^{(i)})}. \quad (1)$$

Here, $f(\cdot)$ denotes the chosen filter (e.g., EnCodec or spectral filtering), and $\mathcal{R}^{(i)} \in \mathbb{R}^F$ is the residual vector for signal $x^{(i)}$. Fig. 2 exemplarily illustrates the EnCodec-based residual fingerprints (RFPs) for four different speech synthesis systems. Each RFP represents the standardized average residual energy distribution across frequencies, computed from the residual spectrograms of 10,480 generated samples. As seen in the figure, the RFP exhibit distinct patterns, highlighting that different synthesis systems leave characteristic traces in the frequency domain. These differences form the basis for discriminating among models in attribution tasks.

D. Scoring and Attribution Criteria

As an alternative to the correlation-based scoring method s_{cor} defined in Section III-C, we propose a scoring method based on the Mahalanobis distance, which accounts for correlations between features. Given a test sample x_{test} , we compare its residual vector $\mathcal{R}_{\text{test}}$ to the fingerprint $\hat{\mathcal{F}}$ via:

$$s_{\text{md}}(\mathcal{R}_{\text{test}}, \hat{\mathcal{F}}) := \sqrt{(\mathcal{R}_{\text{test}} - \hat{\mathcal{F}})^\top \Sigma^{-1} (\mathcal{R}_{\text{test}} - \hat{\mathcal{F}})},$$

where Σ^{-1} is the inverse covariance matrix of the training residuals. Unlike simple correlation scores, this distance normalizes deviations by the feature covariance structure, making it sensitive to model-specific residual patterns even when features are correlated. Such covariance-aware scoring has proven effective in related tasks such as out-of-domain detection (OOD) [53], [54], and here it provides a more robust basis for synthesis model attribution.

Criteria for Single-Model Attribution in an Open-World Setting: To determine whether an audio sample originates from a specific target synthesis system, we perform a binary attribution task by comparing its residual vector $\mathcal{R}_{\text{test}}$ with the target model RFP $\hat{\mathcal{F}}$, obtaining an attribution score based on correlation or Mahalanobis distance. The resulting scores for target-model samples and non-target samples form two distributions, and the Area Under the Receiver Operating Characteristic Curve (AUROC) is computed directly from these score distributions.

Criteria for Multi-Model Attribution in a Closed-World Setting: Attribution is assigned to the model \hat{m} with the closest fingerprints in Mahalanobis distance, where \mathcal{M} denotes the set of available RFPs:

$$\hat{m} = \arg \min_{m \in \mathcal{M}} d_{\text{md}}(\mathcal{R}_{\text{test}}, \hat{\mathcal{F}}_m) \quad (2)$$

V. EVALUATION PROTOCOL

This section describes the experimental setup used to assess the effectiveness, robustness, and reliability of our RFP approach.

A. Datasets

To ensure a comprehensive evaluation of the attribution method across diverse synthesis techniques and deployment scenarios, multiple speech corpora are employed, including synthetic speech generated by a wide range of systems. This setup enables assessment of model attribution performance across different architectures, speakers, languages, and domains. The following subsections describe each benchmark, the types of synthetic speech included, and their relevance for evaluating RFP-based attribution.

1) Augmented LJSpeech Benchmark (English): The LJSpeech corpus [55], a single-speaker English dataset comprising 13,100 audio clips, is used. Synthetic speech samples are drawn from the WaveFake dataset [18] and its extension [56], covering a wide range of synthesis systems. To extend coverage, additional audio is generated using

²EnCodec pretrained model: <https://github.com/facebookresearch/encodec>.

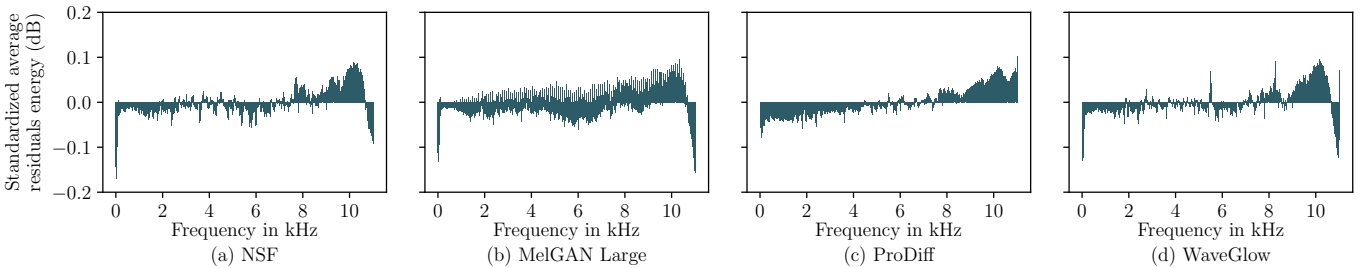


Fig. 2. Extracted fingerprints $\hat{\mathcal{F}}$ from four speech synthesis systems, computed as the average residuals (Equation 1) between the average spectral energy $E_{\bar{x}^{(i)}}$ of generated audio samples and their EnCodec-filtered counterparts $E_{f(x^{(i)})}$, each from 10,480 samples, highlighting model-specific spectral characteristics.

pretrained TTS diffusion-based models (FastDiff³, ProDiff⁴), where LJSpeech transcripts serve as input. For the Hybrid Neural Source-Filter (NSF) approach⁵, a NSF waveform model is trained on the corpus and subsequently employed to generate new speech samples. Each original utterance in LJSpeech is thus paired with a corresponding synthetic version. Together, these systems span four major categories of generative speech technologies. GAN-based models include adversarially trained neural vocoders such as MelGAN Large (MG-L) [57], Parallel WaveGAN (PWG) [58], Multi-band MelGAN (MB-MG) [59], HiFi-GAN (HF-G) [60], Avocado (Avo) [61], and BigVGAN (BVG) [62]. Flow-based models are represented by WaveGlow (WGlow) [38], which generates waveforms through invertible transformations. Diffusion-based models include FastDiff and ProDiff [39], [63], which synthesize speech via iterative denoising. Finally, hybrid models, such as the NSF model [40], combine classical signal processing with neural network components.

2) *JSUT Benchmark (Japanese)*: The JSUT corpus [64], a single-speaker Japanese dataset, is used to evaluate cross-lingual generalization. The basic5000 subcorpus, containing 5,000 utterances, serves as the source of real samples, while synthetic counterparts are obtained from PWG and MB-MelGAN models included in the WaveFake dataset [18].

3) *ASVspoof LA Benchmark (English)*: The ASVspoof 2019 Logical Access (LA) dataset [65], derived from the VCTK [66] corpus, is employed to evaluate attribution in multi-speaker settings. It contains recordings from 107 English speakers, including real speech (*bonafide*) and synthetic speech from 19 TTS and VC systems, totaling approximately 122k utterances. Training and development sets contain samples from a subset of systems, while the evaluation set includes an additional 11 unseen systems, providing a realistic benchmark for multi-speaker model attribution.

4) *CodecFake Benchmark (English and Chinese)*: The CodecFake dataset provides large-scale training, development, and evaluation splits, enabling systematic assessment of attribution under neural codec-specific distortions. It contains

1.06M audio samples, including 132K real recordings from VCTK and AISHELL3 [67] corpora, and 926K synthetic samples generated by seven neural codec-based methods. Unlike other benchmarks, CodecFake focuses on codec-level manipulations and reserves one generation method for testing cross-method generalization.

B. Sample Efficiency

To investigate the impact of training data size on RFP extraction, we experiment with subsets of 70, 80, 90, 100, 110, and the full training set for each benchmark. Attribution is then performed on the full test set, allowing us to assess reliability when only limited model outputs are available.

C. Evasion Attack

Although our main threat model assumes a non-adaptive adversary, we also evaluate a controlled, worst-case evasion scenario to stress-test attribution. We consider a closed-world, multi-model attack in which the adversary—assumed to have full knowledge of the source model’s RFP—modifies a generated sample by subtracting the source RFP and adding a target RFP. Attribution is then assigned to the model m^* with the closest fingerprint in Mahalanobis distance (see Equation 2).

Experiments use the ASVspoof LA and CodecFake benchmarks. For each benchmark, we select 100 random synthetic test samples per category and assign each sample a random target category different from its ground truth. An attack is deemed successful if the manipulated sample is attributed to the chosen target model.

D. Out-of-Domain Detection

For OOD detection, our approach is compared to the recent TADA framework [41], which achieves strong results using a pretrained wav2vec-based self-supervised model combined with k -NN classification ($k = 21$) based on Euclidean distance. In our method, OOD detection is performed by computing the minimal Mahalanobis distance of each sample to the in-domain RFP classes, as defined in Equation 2. A decision threshold is set based on the Equal Error Rate, determined on a validation set containing a balanced mix of in-domain and out-of-domain samples, and then applied to classify the test set.

³FastDiff pretrained model: <https://github.com/Rongjiehuang/FastDiff>.

⁴ProDiff pretrained model: <https://github.com/Rongjiehuang/ProDiff>.

⁵Neural source-filter waveform model: <https://github.com/nii-yamagishilab/project-NN-Pytorch-scripts/tree/master/project/01-nsf>.

E. Data Augmentation for Robustness

To emulate real-world distortions that might affect model attribution, we augment the test set with various audio corruptions. All experiments use the single-model attribution setup.

1) *MP3 Compression*: Each discrete-time input signal $x^{(i)}$ is first compressed and then decoded using the MP3 codec at a specified bitrate. In this study, a standard 128 kbps compression is considered for evaluation. Additionally, a retraining variant is considered, where RFPs are re-estimated using training data augmented with the same MP3 compression.

2) *Echo Effect*: An echo is simulated using a delay-and-add filter. For a discrete-time input signal $x^{(i)}$, the echo-augmented signal $\tilde{x}^{(i)}$ is defined as $\tilde{x}^{(i)}(k) = x^{(i)}(k) + \alpha x^{(i)}(k - D)$, where k is the time index, D is the delay in samples, and $\alpha \in [0, 1]$ controls the echo strength. Robustness is evaluated under two echo strengths ($\alpha = 0.3$ and $\alpha = 0.5$) and two delays (100 ms and 500 ms), corresponding to short and long echo scenarios. Additionally, a retraining variant is considered, where RFPs are re-estimated using training data augmented with the worst-case echo condition ($\alpha = 0.5$, $D = 100$ ms).

3) *Reverberation*: Reverberation is applied using SpeechBrain’s AddReverb module.⁶ Clean utterances are convolved with 26 real room impulse responses from the Type 1 subset of the 2014 Reverberation Challenge dataset [68], simulating the acoustics of small, medium, and large rooms. Additionally, a retraining variant is considered, where RFPs are re-estimated using training data augmented with samples where reberberation is applied.

4) *Background Noise*: To evaluate robustness against additive noise, we use recordings from the MUSAN corpus [68], which contains music, speech, and background noise. Noise augmentation is applied with the SpeechBrain EnvCorrupt module,⁷ using noise parameter values ranging from 10 to 40. Lower values correspond to stronger noise injection, while higher values produce cleaner signals.

VI. PARAMETER TUNING AND FILTER SELECTION

To determine the best filters and STFT configurations, we perform preliminary tuning experiments. These experiments guide the selection of configurations for all subsequent evaluations, including the choice of spectral filters and other hyperparameters. Importantly, none of the samples used in these tuning setups are included in the main evaluation.

A. Spectral Filter Selection

For this, we set aside two synthetic systems from the ASVspoof LA benchmark, A16 and A19. From each system, 95% of the available samples are used to construct RFPs, while the remaining 5% are reserved for validation. Attribution performance is measured pairwise between the 5% source samples and 5% target samples. We evaluate two attribution scoring functions—correlation and Mahalanobis distance—across

⁶AddReverb Speechbrain module: https://speechbrain-anonym.readthedocs.io/en/latest/API/speechbrain.processing.speech_augmentation.html.

⁷EnvCorrupt SpeechBrain module: <https://speechbrain-anonym.readthedocs.io/en/latest/API/speechbrain.lobes.augment.html>.

multiple residual types derived from spectral filters: low-pass and high-pass (cutoffs 1, 3, and 5 kHz) and band-stop and band-pass (bands 4–7 kHz and 5–6 kHz). All residual features are derived from STFT-based acoustic representations with a window size of 8 ms and a hop size of 0.125 ms. Table I summarizes the best-performing configuration from each filter family.

TABLE I
BEST-PERFORMING CONFIGURATIONS FOR EACH SPECTRAL FILTER TYPE ON ASVspoof LA, REPORTING AVERAGE AUROC FOR RFPs A16 AND A19. EVALUATION IS PERFORMED ON THE VALIDATION SET.[†]

Filter type	Correlation		Mahalanobis distance	
	Best config.	Avg. AUROC	Best config.	Avg. AUROC
Low-pass	3 kHz cutoff	0.92	1 kHz cutoff	0.98
High-pass	1 kHz cutoff	0.76	5 kHz cutoff	0.95
Band-stop	4–7 kHz stop	0.67	4–7 kHz stop	0.94
Band-pass	5–6 kHz pass	0.93	5–6 kHz pass	0.98

[†]Bold highlights top results selected for subsequent evaluations.

Filter choice: The 1 kHz low-pass and 5–6 kHz band-pass filters achieve the highest AUROC, indicating that synthesis artifacts are present in both low- and mid-frequency bands. Mahalanobis distance consistently outperforms correlation, as it accounts for the covariance structure of residual features and can better detect subtle, correlated variations in audio signals. These two filters with Mahalanobis distance are therefore used for all subsequent spectral filtering experiments. Detailed pairwise AUROC results for all spectral filters and all target systems on this validation set are provided in App. IX-A.

B. Effect of STFT Settings

Beyond filter choice, attribution may also depend on the time–frequency resolution of the STFT. We therefore compare two settings: a small window size of 8 ms with a high overlap of 0.125 ms, and a commonly used configuration in speech processing with a window size of 25 ms and a hop size of 10 ms. Table II reports the average Mahalanobis-based attribution AUROC scores across multiple benchmarks using the selected spectral filters (1 kHz low-pass and 5–6 kHz band-pass). The configuration with the smaller window and shorter

TABLE II
COMPARISON OF SINGLE-MODEL ATTRIBUTION AUROC SCORES ACROSS BENCHMARKS FOR TWO SPECTRAL SETTINGS WITH MAHALANOBIS DISTANCE; EACH CELL SHOWS LOW-PASS 1 kHz / BAND-PASS 5–6 kHz SCORES. EVALUATION IS PERFORMED ON THE VALIDATION SET.

Setting [†]	LJSpeech	ASVspoof LA	CodecFake	JSUT
WS=8 ms, HL=0.125 ms	1.00 / 1.00	0.99 / 0.99	0.98 / 0.98	1.00 / 1.00
WS=25 ms, HL=10 ms	1.00 / 0.99	0.95 / 0.97	0.98 / 0.98	1.00 / 1.00

[†]WS = Window Size. HL = Hop Length.

hop size consistently achieves slightly higher AUROC scores across all benchmarks, particularly for ASVspoof LA and LJSpeech benchmarks, compared to the 25 ms / 10 ms setting. This indicates that a finer temporal sampling better captures synthesis artifacts, improving attribution performance. Based on this, we adopt the 8 ms / 0.125 ms STFT configuration for all subsequent experiments. Detailed pairwise AUROC results for the 25 ms / 10 ms configuration are provided in App. IX-B,

while pairwise results for the adopted setting are reported in the following section VII-A2.

VII. EVALUATION AND RESULTS

Using the filters and STFT configuration from Section VI, we evaluate single-model attribution on the main benchmarks: Augmented LJSpeech, JSUT, ASVspoof LA, and CodecFake. The attribution task compares residual vectors from unseen samples to the target system’s RFP using Mahalanobis distance. Each experiment is repeated five times to account for variability due to stochastic processes in the models (e.g., random initialization or sampling), and we report the average results across runs. In all cases, the test sets consist of unseen real and synthetic samples to reliably assess generalization performance. The code, pre-trained models, filter coefficients, and synthetic audio samples used in our experiments are available at <https://github.com/blindconf/fingerprint>.

A. Single-Model Attribution in an Open-World Setting

1) *Experimental Setup*: We split the dataset into 80% for training, 10% for validation, and 10% for testing. To ensure fair comparison across conditions, we construct balanced sets, where each category contributes the same number of samples. For the larger CodecFake dataset, we subsample in such a way that the training, validation, and test partitions match the size of those in the augmented LJSpeech benchmark. To determine whether an audio sample originates from a specific target synthesis system, we perform a binary attribution task by comparing residual vectors $\mathcal{R}_{\text{test}}$ with the known model RFP $\hat{\mathcal{F}}$. We report the AUROC to quantify attribution performance.

2) *Attribution Results*: The goal of our evaluation is to assess how well the RFP enables discrimination between the target system’s outputs and those from all other sources (including real speech). Overall, the RFP demonstrates strong discriminative power, achieving near-perfect AUROC scores across a wide range of synthetic and voice-converted speech systems.

Augmented LJSpeech & JSUT Benchmarks: Across most sources and targets, the RFP achieves perfect separation, with AUROC values consistently reaching 1.0. Tables XVIII and XX in App. IX-B summarize these results, demonstrating that the RFP remains both highly reliable and effective under these conditions.

ASVspoof LA Benchmark: The RFP achieves near-perfect attribution for most systems, highlighting its generalizability. Table III shows AUROC scores for all target–source pairs. A few cases show slightly lower scores. For example, both A01 and A04 are TTS systems that share short-term acoustic patterns such as cepstral, Mel-warped, and spectral-envelope features used by their waveform generators, yielding an AUROC of 0.86 / 0.87. Similarly, A06 and A04 both rely on explicit waveform manipulations rather than purely neural synthesis, and both use MFCCs, which may explain the lower separation (0.77 / 0.74). Finally, A02 and A03 are closely related TTS systems that employ the same waveform generator (WORLD) and acoustic features, resulting in an

AUROC of 0.79 / 0.82. These slight reductions are likely due to inherent similarities between certain systems rather than any shortcoming of the RFP. Nevertheless, the RFP continues to accurately distinguish nearly all sources (including real speech) across different input types (VC, TTS, or hybrid), demonstrating its robustness even in challenging open-world attribution scenarios.

TABLE III

SINGLE-MODEL ATTRIBUTION AUROC SCORES ON ASVspoof LA WITH THE 8 MS WINDOW SIZE / 0.125 MS HOP LENGTH STFT CONFIGURATION AND MAHALANOBIS DISTANCE. ROWS: SOURCES; COLUMNS: TARGETS. CELLS: SCORES FOR LOW-PASS 1 KHZ / BAND-PASS 5–6 KHZ FILTERS.[†]

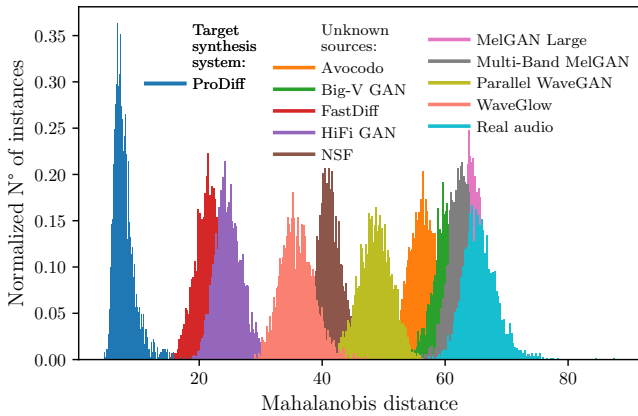
Source\Target	A01	A02	A03	A04	A05*	A06*
A01	-	1.00 / 1.00	1.00 / 1.00	0.86 / 0.87	1.00 / 1.00	1.00 / 1.00
A02	1.00 / 1.00	-	0.79 / 0.82	1.00 / 1.00	0.93 / 0.92	1.00 / 1.00
A03	1.00 / 1.00	1.00 / 1.00	-	1.00 / 1.00	1.00 / 0.99	1.00 / 1.00
A04	0.96 / 0.98	1.00 / 1.00	1.00 / 1.00	-	1.00 / 1.00	1.00 / 1.00
A05*	1.00 / 1.00	1.00 / 0.99	0.96 / 0.93	1.00 / 1.00	-	1.00 / 1.00
A06*	0.97 / 0.94	1.00 / 1.00	1.00 / 1.00	0.77 / 0.74	1.00 / 1.00	-
A07	0.99 / 0.94	1.00 / 1.00	1.00 / 1.00	0.94 / 0.90	1.00 / 1.00	1.00 / 1.00
A08	1.00 / 1.00	1.00 / 1.00	1.00 / 1.00	1.00 / 1.00	1.00 / 1.00	1.00 / 1.00
A09	1.00 / 1.00	1.00 / 1.00	0.93 / 0.93	1.00 / 1.00	0.99 / 0.99	1.00 / 1.00
A10	1.00 / 1.00	1.00 / 1.00	0.98 / 0.97	1.00 / 1.00	1.00 / 0.99	1.00 / 1.00
A11	1.00 / 1.00	1.00 / 1.00	1.00 / 1.00	1.00 / 1.00	1.00 / 1.00	1.00 / 1.00
A12	1.00 / 1.00	1.00 / 1.00	1.00 / 0.99	1.00 / 1.00	1.00 / 1.00	1.00 / 1.00
A13‡	1.00 / 1.00	1.00 / 1.00	1.00 / 0.99	1.00 / 1.00	1.00 / 1.00	1.00 / 1.00
A14‡	1.00 / 1.00	1.00 / 1.00	1.00 / 1.00	1.00 / 1.00	1.00 / 1.00	1.00 / 1.00
A15‡	1.00 / 1.00	1.00 / 1.00	0.98 / 0.97	1.00 / 1.00	1.00 / 0.98	1.00 / 1.00
A17*	1.00 / 1.00	1.00 / 1.00	0.97 / 0.99	1.00 / 1.00	0.99 / 0.96	1.00 / 1.00
A18*	1.00 / 1.00	1.00 / 1.00	0.99 / 0.94	0.99 / 1.00	1.00 / 1.00	1.00 / 1.00
Bonafide	1.00 / 1.00	1.00 / 1.00	0.99 / 0.99	1.00 / 1.00	1.00 / 0.99	1.00 / 1.00
Avg.	1.00 / 0.99	1.00 / 1.00	0.97 / 0.97	0.97 / 0.97	1.00 / 0.99	1.00 / 1.00

* VC systems; ‡ TTS+VC; unmarked: TTS only. Higher AUROC values = better separation.

CodecFake Benchmark: The RFP achieves consistently high AUROC scores across nearly all source-target neural codec pairs, as shown in Table IV, with most comparisons—including real speech—reaching an AUROC of 1.0, indicating perfect or near-perfect attribution. Only a few source-target neural codec combinations, such as C2 and C6 (0.79 / 0.89) and C7 and C6 (0.75 / 0.82), show lower separability. These cases can be attributed to similarities in codec architecture and quantization strategy. Specifically, C2 (SpeechTokenizer) and C6 (AcademicCodec) both employ residual vector quantization (RVQ) mechanisms, producing acoustically similar patterns in certain frequency bands. C7 (Descript-audio-codec), which spans a wide frequency range and uses enhanced RVQ with periodic activations, may also partially overlap with features of C6. Despite these minor overlaps, the AUROC values remain high, demonstrating that the RFP effectively captures codec-specific characteristics.

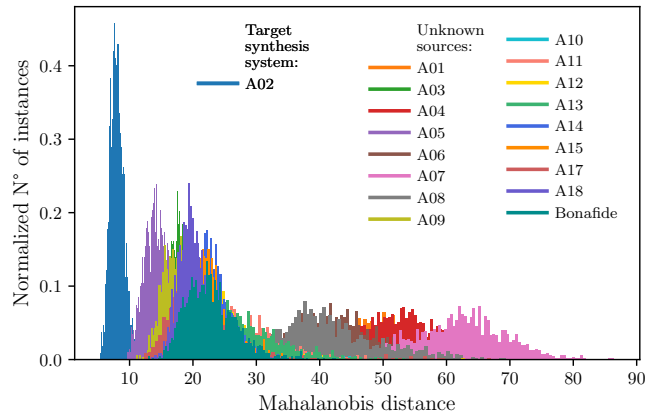
These overall results show that our FPR approach enables near-perfect attribution of synthetic speech to its source, even for highly similar models, while reliably distinguishing real from synthetic speech. As an example, Fig. 3 shows the s_{md} between a target system’s RFP and various unseen inputs, including real audio, samples from other synthesis systems, and samples from the target system itself.

3) *EnCodec vs. Spectral Filters*: We evaluate the performance of EnCodec-based residuals by comparing them with the selected spectral filters. As shown in Table V, spectral filters achieve a higher average AUROC (0.99) than EnCodec (0.95 / 0.93). The lower performance of EnCodec on CodecFake is likely due to the presence of samples generated by the EnCodec encoder itself, which reduces residual discrim-



(a) ProDiff model attribution: Assessment by scoring unseen inputs from various sources with Mahalanobis distance, including samples generated by the ProDiff model itself, using the augmented LJSpeech benchmark.

Fig. 3. Single-model attribution results in an open-world setting for two target synthesis systems: (a) ProDiff and (b) A02. In both cases, lower distances indicate that a sample is more likely to stem from the corresponding target system.



(b) A02 model attribution: Assessment by scoring unseen inputs from various sources with Mahalanobis distance, including samples generated by the A02 model itself, using the ASVspoof LA benchmark.

TABLE IV

SINGLE-MODEL ATTRIBUTION AUROC SCORES ON CODECFAKE WITH THE 8 MS WINDOW SIZE / 0.125 MS HOP LENGTH STFT CONFIGURATION AND MAHALANOBIS DISTANCE. ROWS: SOURCES; COLUMNS: TARGETS. CELLS: SCORES FOR LOW-PASS 1 KHZ / BAND-PASS 5–6 KHZ FILTERS.[†]

Source\Target	C1	C2	C3	C4	C5	C6
C1	-	1.00 / 1.00	1.00 / 1.00	1.00 / 1.00	1.00 / 1.00	1.00 / 1.00
C2	1.00 / 0.99	-	1.00 / 1.00	0.99 / 0.99	0.99 / 1.00	0.79 / 0.89
C3	1.00 / 1.00	1.00 / 1.00	-	1.00 / 1.00	1.00 / 1.00	1.00 / 1.00
C4	1.00 / 1.00	1.00 / 1.00	1.00 / 1.00	-	1.00 / 1.00	0.99 / 0.99
C5	1.00 / 1.00	0.96 / 0.95	1.00 / 1.00	0.99 / 0.99	-	0.91 / 0.94
C6	1.00 / 0.99	0.87 / 0.87	1.00 / 1.00	0.99 / 0.99	0.99 / 0.99	-
C7	1.00 / 1.00	0.93 / 0.95	1.00 / 1.00	0.99 / 0.99	1.00 / 1.00	0.75 / 0.82
Real	1.00 / 1.00	0.96 / 0.98	1.00 / 1.00	0.99 / 0.99	1.00 / 1.00	0.88 / 0.93
Avg.	1.00 / 1.00	0.96 / 0.96	1.00 / 1.00	0.99 / 0.99	1.00 / 1.00	0.90 / 0.94

[†] Higher AUROC values = better separation between the target system and all other sources.

inability. In contrast, spectral filtering isolates frequency regions where synthesis artifacts concentrate, offering a simple, interpretable, and competitive alternative. Detailed EnCodec results are reported in App. IX-C.

TABLE V

COMPARISON OF SINGLE-MODEL ATTRIBUTION AUROC SCORES: ENCODEC (CORRELATION / MAHALANOBIS) VS. SPECTRAL FILTERS (MAHALANOBIS), AVERAGED ACROSS BENCHMARKS.

Benchmark	EnCodec	Low-pass 1 kHz	Band-pass 5–6 kHz
LJSpeech	0.99 / 0.95	1.00	1.00
JSUT	1.00 / 1.00	1.00	1.00
ASVspoof LA	0.95 / 0.89	0.99	0.99
CodecFake	0.85 / 0.86	0.98	0.98
Avg.	0.95 / 0.93	0.99	0.99

B. Sample Efficiency

Attribution performance averages across all source–target pairs for single-model attribution. Table VI presents the accuracy achieved on each benchmark for different subset sizes. The results indicate that attribution remains robust even with limited training data. Augmented LJSpeech benchmark achieves near-perfect accuracy with only 70 samples and maintains an AUROC score of 1.00 from 80 samples onward.

JSUT improves steadily from 0.96 at 70 samples to 1.00 at 100 samples. Even for the more challenging ASVspoof LA and CodecFake benchmarks, stable performance is obtained with just 90 samples, achieving 0.98 and 0.95. Overall, fewer than 100 training samples per benchmark provide reliable RFP extraction. This finding is especially relevant for single-model attribution, where defenders may have only partial access to target outputs. In realistic adversarial scenarios—for example, when attackers deploy privately trained or unreleased models—collecting a large number of samples may be difficult. Our results suggest that attribution remains feasible under such constraints. On an NVIDIA A40 GPU with 48 GB, fingerprint extraction for the LJSpeech benchmark requires 1.52 s for 100 samples and 153.3 s for the full 10,480-sample training set, while per-sample attribution takes only 0.015 s. The computational complexity is $O(N \cdot d^2)$ for extraction, and $O(d^2)$ for attribution, where N is the number of training samples and d is the RFP dimensionality. These results demonstrate that our method is lightweight and scalable.

TABLE VI
SINGLE-MODEL ATTRIBUTION AUROC SCORES ON TRAINING SUBSETS (AVERAGE ACROSS SOURCE–TARGET PAIRS) WITH 1 KHZ LOW-PASS FILTER, 8 MS/0.125 MS STFT AND MAHALANOBIS DISTANCE.[†]

Benchmark	70	80	90	100	110	Full
Augmented LJSpeech	0.98	1.00	1.00	1.00	1.00	1.00
JSUT	0.96	0.98	0.99	1.00	1.00	1.00
ASVspoof LA	0.92	0.97	0.98	0.98	0.98	0.99
CodecFake	0.92	0.95	0.95	0.96	0.97	0.98

[†] Column headers indicate training samples for fingerprint extraction.

C. Evasion Attack

Our evasion attack achieves limited success on both benchmarks. On ASVspoof LA (categories A1–A6), the attack reaches an overall accuracy of 0.41. Its performance is higher on the CodecFake benchmark (categories C1–C6), where it attains an accuracy of 0.70. These findings indicate that

reliably manipulating a sample to be attributed to a target model remains challenging, even when the attacker has full knowledge of the source RFP.

D. Data Augmentation for Robustness

RFPs are evaluated under common audio post-processing transformations. The evaluation considers an extended test set that includes corrupted data. In addition, in a retraining variant, RFPs are re-estimated on the corrupted data as a light fine-tuning step.

1) *MP3 Compression*: The results are summarized in Table VII, reporting the average single-model attribution AUROC scores across benchmarks, using Mahalanobis distance. Compression at 128 kbps degrades attribution performance, particularly for JSUT and ASVspoof LA, where AUROC drops to 0.57–0.64. Retraining RFPs on training data augmented with 128 kbps MP3 compression (Table VII, last row) substantially restores performance across all datasets, with AUROC values returning close to baseline. These findings indicate that MP3 compression can challenge attribution performance, but retraining with compressed data effectively mitigates the degradation.

TABLE VII

AVERAGE SINGLE-MODEL ATTRIBUTION AUROC SCORES ACROSS BENCHMARKS WITH 1 KHZ LOW-PASS FILTER, 8 MS/0.125 MS STFT AND MAHALANOBIS DISTANCE. CORRUPTION: MP3 COMPRESSION.

MP3 compression	LJSpeech	JSUT	ASVspoof	CodecFake
No effect	1.00	1.00	0.99	0.98
128 kbps	0.63	0.57	0.64	0.79
RFP retrained [†]	0.99	1.00	0.97	0.98

[†] Retrained on training data with MP3 compression at 128 kbps.

2) *Echo Effect*: The results are summarized in Table VIII, which reports the overall average pairwise AUROC across benchmarks. Mild echo conditions (e.g., $\alpha = 0.3$) have only a limited impact, with AUROC values remaining above 0.95 for most datasets. More severe settings (e.g., $\alpha = 0.5$ with short delay) cause larger degradation, particularly for JSUT and CodecFake, where AUROC drops to 0.92. The retraining condition (Table VIII, last row) shows that incorporating echo-augmented training data to extract RFP maintains high attribution performance even under the worst distortions. These findings indicate that attribution fingerprints are resilient to moderate echo effects, while severe echoes can slightly reduce performance. Retraining with echo-augmented data provides an additional step to sustain high performance under such challenging conditions.

3) *Reverberation*: Results are summarized in Table IX, reporting the average single-model attribution AUROC across benchmarks. Reverberation reduces attribution performance compared to clean conditions, with AUROC values dropping to 0.64–0.84 across datasets. Retraining RFPs on training data augmented with reverberation (Table IX, last row) improves robustness, partially restoring performance toward baseline levels. These results indicate that while reverberation presents

TABLE VIII
AVERAGE SINGLE-MODEL ATTRIBUTION AUROC SCORES ACROSS BENCHMARKS WITH 1 KHZ LOW-PASS FILTER, 8 MS/0.125 MS STFT AND MAHALANOBIS DISTANCE. CORRUPTION: ECHO EFFECT.

Echo effect	LJSpeech	JSUT	ASVspoof	CodecFake
No effect	1.00	1.00	0.99	0.98
$\alpha = 0.3, D = 100$ ms	1.00	0.98	0.96	0.95
$\alpha = 0.3, D = 500$ ms	1.00	0.99	0.96	0.92
$\alpha = 0.5, D = 100$ ms	0.98	0.92	0.92	0.92
$\alpha = 0.5, D = 500$ ms	0.99	0.95	0.95	0.94
RFP retrained [†]	1.00	1.00	0.99	0.98

[†] Retrained on training data with worst-case echo ($\alpha = 0.5, D = 100$ ms).

a challenge for attribution, retraining with reverberation-augmented data helps maintain relatively high attribution performance across all benchmarks.

TABLE IX
AVERAGE SINGLE-MODEL ATTRIBUTION AUROC SCORES ACROSS BENCHMARKS WITH 1 KHZ LOW-PASS FILTER, 8 MS/0.125 MS STFT AND MAHALANOBIS DISTANCE. CORRUPTION: REVERBERATION.

Effect	LJSpeech	JSUT	ASVspoof	CodecFake
No effect	1.00	1.00	0.99	0.98
Reverberation	0.65	0.64	0.81	0.84
RFP retrained [†]	0.97	0.96	0.91	0.92

[†] Retrained on training data with reverberation.

4) *Background Noise*: Since the EnvCorrupt noise parameters (10–40) are not directly interpretable in terms of distortion severity, we report the corresponding average signal-to-noise ratio (SNR) in dB for each setting. The SNR indicates how strong the speech signal is relative to the added noise: lower values mean heavier corruption, while higher values correspond to cleaner signals. Table X shows that attribution remains highly reliable even under strong noise. At the lowest SNR level (9.56 dB), performance is still strong with AUROC = 0.89, where speech is noticeably degraded [69]. Accuracy steadily improves with cleaner signals, reaching near-perfect AUROC (≥ 0.98) once the SNR exceeds 32 dB. These findings demonstrate that our RFP preserves discriminability in noisy environments, degrading gracefully under extreme corruption.

E. Multi-Model Attribution in a Closed-World Setting

Closed-world attribution is evaluated across datasets using the data splits described in Section VII-A1. The number of fixed candidate models per benchmark is 10 for augmented LJSpeech, 2 for JSUT, 6 for ASVspoof LA, and 6 for CodecFake. We evaluate two RFP-based model classifiers, each differing in the way the classifier is implemented.

TABLE X
AVERAGE SINGLE-MODEL ATTRIBUTION AUROC SCORES UNDER BACKGROUND NOISE CORRUPTION ON THE AUGMENTED LJSPEECH BENCHMARK.

Noise param [†]	10	15	20	25	30	35	40
Avg. SNR dB	9.56	13.57	17.96	22.60	27.40	32.28	37.22
AUROC	0.89	0.92	0.94	0.96	0.97	0.98	0.99

[†] SpeechBrain EnvCorrupt noise parameter values.

RFP: This classifier does not require any neural network training; for each test sample, the attribution label is assigned to the synthesis system whose precomputed residual fingerprint has the minimum Mahalanobis distance w.r.t. the residual features of the test sample (see Equation 2). We use our precomputed RFPs derived from low-pass filtered residual features that achieved the best single-model attribution (see Table VI).

RFP CNN: This classifier adopts a compact residual CNN with squeeze-and-excitation modules, trained directly on residual features. Residuals are extracted with a 1 kHz low-pass filter and an STFT using 25 ms windows and 10 ms hop size. The network applies three convolutional blocks with increasing channel sizes (32, 64, and 128), each including a residual connection, batch normalization, and ReLU activations, allowing the model to exploit local structure in the residual features.

We compare these models against four baselines that have demonstrated strong performance in synthetic speech detection, each adapted to our multi-model attribution task: X-vector [70], LCNN [71], ResNet [72], and SE-ResNet [73]. All models except RFP are trained for 10 epochs using Adam (learning rate 0.001, $\beta = (0.9, 0.98)$) with a linear scheduler and 100 warm-up iterations, using cross-entropy loss with softmax outputs. The final prediction corresponds to the class with the highest probability. Additional details on baseline architectures are provided in App. IX-D. We report accuracy and F1-score averaged over five independent runs, evaluation is balanced by using the same number of samples per class. Table XI shows that our RFP based classifiers outperform or match strong baselines across benchmarks. The RFP classifier, albeit its simplicity, achieves perfect accuracy on Augmented LJSpeech and JSUT, and near-perfect scores on ASVspoof (0.97) and CodecFake (0.99). The RFP CNN outperforms all other models, demonstrating that a simple CNNs trained on residual features can match or exceed the performance of notably larger baseline models with minimal training. The results show that residual fingerprints provide highly discriminative cues even without training. Additional metrics, including precision and recall, are reported in App. IX-E.

TABLE XI

CLOSED-WORLD MULTI-MODEL ATTRIBUTION PERFORMANCE OF RFP CLASSIFIERS COMPARED TO BASELINES ACROSS BENCHMARKS. CELLS: ACCURACY / F1 SCORE, AVG. OVER 5 RUNS WITH 10 EPOCHS EACH.

Model	Augm. LJSpeech	JSUT	ASVspoof	CodecFake
X-vector	0.99 / 0.99	0.99 / 0.99	1.00 / 1.00	1.00 / 1.00
LCNN	0.98 / 0.98	0.98 / 0.98	1.00 / 1.00	0.98 / 0.98
ResNet	0.98 / 0.98	0.99 / 0.99	1.00 / 1.00	1.00 / 1.00
SE-ResNet	0.98 / 0.98	1.00 / 1.00	1.00 / 1.00	1.00 / 1.00
RFP (ours)	1.00 / 1.00	1.00 / 1.00	0.97 / 0.97	0.99 / 0.99
RFP CNN (ours)	1.00 / 1.00	1.00 / 1.00	1.00 / 1.00	1.00 / 1.00

F. Real vs. Synthetic Classification

This binary classification task uses the same data splits described in Section VII-A1. We evaluate generalization to unseen samples, particularly in the ASVspoof LA and CodecFake, which contain 11 and 1 unseen categories, respectively,

during training. We report accuracy and F1-score averaged over five independent runs. To maintain class balance, real speech samples are oversampled to match the number of synthetic ones. All models from Section VII-E are re-trained with binary cross-entropy loss. Logits are passed through a sigmoid function, and predictions are thresholded at 0.5. Table XII compares our RFP CNN classifier to baselines, which by leveraging local structure in residual spectrograms, achieves perfect accuracy on Augmented LJSpeech and JSUT, and strong performance on ASVspoof (0.95) and CodecFake (0.94), highlighting the effectiveness of residual fingerprints even in lightweight models. Additional metrics, including precision, recall, and standard-deviation are reported in App. IX-F.

TABLE XII

REAL VS. SYNTHETIC CLASSIFICATION PERFORMANCE OF OUR RFP CNN COMPARED TO BASELINES ACROSS BENCHMARKS. CELLS: ACCURACY / F1 SCORE, AVG. OVER 5 RUNS WITH 10 EPOCHS OF TRAINING EACH.

Model	Augm. LJSpeech	JSUT	ASVspoof	CodecFake
X-vector	0.91 / 0.92	1.00 / 1.00	0.87 / 0.86	0.93 / 0.93
LCNN	0.96 / 0.96	0.99 / 0.99	0.93 / 0.93	0.93 / 0.93
ResNet	0.98 / 0.98	1.00 / 1.00	0.95 / 0.94	0.94 / 0.93
SE-ResNet	0.98 / 0.98	1.00 / 1.00	0.95 / 0.94	0.94 / 0.93
RFP CNN (ours)	1.00 / 1.00	1.00 / 1.00	0.95 / 0.95	0.94 / 0.93

G. Out-of-domain Detection

Following TADA’s experimental setup with the ASVspoof LA dataset—where A01–A06 are treated as in-domain, five unseen systems are used for validation, and six unseen systems are held out for testing—our method achieves an F1-score of 0.91, compared to 0.86 for TADA. This demonstrates that, even with a simple training-free OOD detection via RFP extraction, our green AI approach outperforms the recent self-supervised TADA framework.

VIII. CONCLUSION

With modern speech generation achieving high realism, detecting and attributing synthetic audio is critical for secure voice systems and forensic applications. Our RFP approach extracts model-specific artifacts from low- or band-pass residuals, offering a compact, training-free, and environmentally efficient solution that works with fewer than 100 samples. RFPs achieve near-perfect AUROC in open-world attribution, effectively separate real from synthetic speech, and provide discriminative cues in closed-world multi-model attribution, often matching deeper networks. Extensive tests across languages, synthesis paradigms, and realistic audio distortions show robust performance, which can be further improved via simple data augmentation. These results demonstrate RFPs’ practicality for rapid-response detection, content moderation, and scalable forensic pipelines, with future work exploring cross-lingual fingerprints, alternative decompositions, fingerprint ensembles, and extreme perturbations.

REFERENCES

[1] B. Yan, J. Shi, Y. Tang, H. Inaguma, Y. Peng, S. Dalmia, P. Polák, P. Fernandes, D. Berrebbi, T. Hayashi, X. Zhang, Z. Ni, M. Hira, S. Maiti, J. Pino, and S. Watanabe, "ESPNet-ST-v2: Multipurpose spoken language translation toolkit," in *Proceedings of the 61st Annual Meeting of the Association for Computational Linguistics (Volume 3: System Demonstrations)*. Association for Computational Linguistics, 2023, pp. 400–411.

[2] M. Ravanelli, T. Parcollet, A. Moumen, S. de Langen, C. Subakan, P. Plantinga, Y. Wang, P. Mousavi, L. D. Libera, A. Ploujnikov, F. Paissan, D. Borra, S. Zaiem, Z. Zhao, S. Zhang, G. Karakasidis, S.-L. Yeh, P. Champion, A. Rouhe, R. Braun, F. Mai, J. Zuluaga-Gomez, S. M. Mousavi, A. Nautsch, X. Liu, S. Sagar, J. Duret, S. Mdhaaffar, G. Laperrriere, M. Rouvier, R. D. Mori, and Y. Esteve, "Open-source conversational AI with speechbrain 1.0," 2024.

[3] S. L. Metzger, K. T. Littlejohn, A. B. Silva, D. A. Moses, M. P. Seaton, R. Wang, M. E. Dougherty, J. R. Liu, P. Wu, M. A. Berger, I. Zhuravleva, A. Tu-Chan, K. Ganguly, G. K. Anumanchipalli, and E. F. Chang, "A high-performance neuroprosthesis for speech decoding and avatar control," *Nature*, vol. 620, pp. 1037–1046, 2023.

[4] R. Badlani, R. Valle, K. J. Shih, J. F. Santos, S. Gururani, and B. Catanzaro, "RAD-MMM: Multilingual Multiaccented Multispeaker Text To Speech," in *Proc. Interspeech*, 2023, pp. 626–630.

[5] N. Bontridder and Y. Poulet, "The role of artificial intelligence in disinformation," *Data N°38; Policy*, vol. 3, p. e32, 2021.

[6] P. Gupta, H. A. Patil, and R. C. Guido, "Vulnerability issues in automatic speaker verification (ASV) systems," *EURASIP Journal on Audio, Speech, and Music Processing*, vol. 10, 2024.

[7] R. A. Delfino, "Deepfakes on trial: A call to expand the trial judge's gatekeeping role to protect legal proceedings from technological fakery," *Hastings Law Journal*, vol. 74, no. 2, p. 293, 2023.

[8] D. Dai, Y. Chen, L. Chen, M. Tu, L. Liu, R. Xia, Q. Tian, Y. Wang, and Y. Wang, "Cloning one's voice using very limited data in the wild," in *ICASSP 2022 - 2022 IEEE International Conference on Acoustics, Speech and Signal Processing (ICASSP)*, 2022, pp. 8322–8326.

[9] K. Klapsas, N. Ellinas, K. Nikitaras, G. Vamvoukakis, P. Kakoulidis, K. Markopoulos, S. Raptis, J. S. Sung, G. Jho, A. Chalamandaris, and P. Tsiakoulis, "Self supervised learning for robust voice cloning," in *Proc. Interspeech*, 2022, pp. 4935–4939.

[10] X. Wang, H. Delgado, H. Tak, J.-w. Jung, H.-j. Shim, M. Todisco, I. Kukanov, X. Liu, M. Sahidullah, T. Kinnunen, N. Evans, K. A. Lee, and J. Yamagishi, "ASVspoof 5: Crowdsourced speech data, deepfakes, and adversarial attacks at scale," in *ASVspoof Workshop*, 2024.

[11] J. Yi, J. Tao, R. Fu, X. Yan, C. Wang, T. Wang, C. Y. Zhang, X. Zhang, Y. Zhao, Y. Ren, L. Xu, J. Zhou, H. Gu, Z. Wen, S. Liang, Z. Lian, S. Nie, and H. Li, "ADD 2023: the second audio deepfake detection challenge," in *DADA@IJCAI*, 2023.

[12] B. News. (2025) Imposter used AI to pose as Marco Rubio and contact foreign ministers. Last visited: 2025-09-14. [Online]. Available: <https://www.bbc.com/news/articles/crrqkyyjewno>

[13] X. Yan, J. Yi, J. Tao, C. Wang, H. Ma, T. Wang, S. Wang, and R. Fu, "An initial investigation for detecting vocoder fingerprints of fake audio," in *Proceedings of the 1st International Workshop on Deepfake Detection for Audio Multimedia*, ser. DDAM '22. New York, NY, USA: Association for Computing Machinery, 2022, p. 61–68.

[14] J. Deng, Y. Ren, T. Zhang, H. Zhu, and Z. Sun, "VFD-Net: Vocoder Fingerprints Detection for Fake Audio," in *ICASSP*, 2024, pp. 12 151–12 155.

[15] Y. Wang, R. Skerry-Ryan, D. Stanton, Y. Wu, R. J. Weiss, N. Jaitly, Z. Yang, Y. Xiao, Z. Chen, S. Bengio, Q. Le, Y. Agiomyrgiannakis, R. Clark, and R. A. Saurous, "Tacotron: Towards End-to-End Speech Synthesis," in *Proc. Interspeech 2017*, 2017, pp. 4006–4010.

[16] T. Kaneko, H. Kameoka, K. Hiramatsu, and K. Kashino, "Sequence-to-Sequence Voice Conversion with Similarity Metric Learned Using Generative Adversarial Networks," in *Interspeech 2017*, 2017, pp. 1283–1287.

[17] Y. Lu, Y. Xie, R. Fu, Z. Wen, J. Tao, Z. Wang, X. Qi, X. Liu, Y. Li, Y. Liu, X. Wang, and S. Shi, "Codecfake: An Initial Dataset for Detecting LLM-based Deepfake Audio," in *Interspeech 2024*, 2024, pp. 1390–1394.

[18] J. Frank and L. Schönherr, "WaveFake: A Data Set to Facilitate Audio Deepfake Detection," in *Thirty-fifth Conference on Neural Information Processing Systems Datasets and Benchmarks Track*, 2021.

[19] F. Li, Y. Chen, H. Liu, Z. Zhao, Y. Yao, and X. Liao, "Vocoder Detection of Spoofing Speech Based on GAN Fingerprints and Domain Generalization," *ACM Trans. Multimedia Comput. Commun. Appl.*, vol. 20, no. 6, mar 2024.

[20] Nicolas Müller and Franziska Diekmann and Jennifer Williams, "Attacker Attribution of Audio Deepfakes," in *Interspeech 2022*, 2022, pp. 2788–2792.

[21] X. Zhou, D. Garcia-Romero, R. Duraiswami, C. Espy-Wilson, and S. Shamma, "Linear versus mel frequency cepstral coefficients for speaker recognition," in *2011 IEEE Workshop on Automatic Speech Recognition & Understanding*, 2011, pp. 559–564.

[22] M. Todisco, H. Delgado, and N. Evans, "Constant Q cepstral coefficients: A spoofing countermeasure for automatic speaker verification," *Computer Speech & Language*, vol. 45, pp. 516–535, 2017.

[23] J. Li, H. Wang, P. He, S. M. Abdullahi, and B. Li, "Long-term variable Q transform: A novel time-frequency transform algorithm for synthetic speech detection," *Digital Signal Processing*, vol. 120, p. 103256, 2022.

[24] Z. Ji, Z.-Y. Li, P. Li, M. An, S. Gao, D. Wu, and F. Zhao, "Ensemble Learning for Countermeasure of Audio Replay Spoofing Attack in ASVspoof2017," in *Proc. Interspeech*, 2017, pp. 87–91.

[25] D. Snyder, D. Garcia-Romero, A. McCree, G. Sell, D. Povey, and S. Khudanpur, "Spoken Language Recognition using X-vectors," in *The Speaker and Language Recognition Workshop*, 2018.

[26] Z. Wu, R. K. Das, J. Yang, and H. Li, "Light Convolutional Neural Network with Feature Genuinization for Detection of Synthetic Speech Attacks," in *Proc. Interspeech*, 2020, pp. 1101–1105.

[27] A. Chinthia, B. Thai, S. J. Sohrawardi, K. Bhatt, A. Hickerson, M. Wright, and R. Ptucha, "Recurrent convolutional structures for audio spoof and video deepfake detection," *IEEE Journal of Selected Topics in Signal Processing*, vol. 14, no. 5, pp. 1024–1037, 2020.

[28] M. Alzantot, Z. Wang, and M. B. Srivastava, "Deep Residual Neural Networks for Audio Spoofing Detection," in *Proc. Interspeech*, 2019, pp. 1078–1082.

[29] Y. Yang, H. Wang, H. Dinkel, Z. Chen, S. Wang, Y. Qian, and K. Yu, "The SJTU Robust Anti-Spoofing System for the ASVspoof 2019 Challenge," in *Proc. Interspeech 2019*, 2019, pp. 1038–1042.

[30] J. Kim and S. M. Ban, "Phase-aware spoof speech detection based on Res2net with phase network," in *ICASSP 2023 - 2023 IEEE International Conference on Acoustics, Speech and Signal Processing (ICASSP)*, 2023, pp. 1–5.

[31] C.-I. Lai, N. Chen, J. Villalba, and N. Dehak, "ASSERT: Anti-Spoofing with Squeeze-Excitation and Residual Networks," in *Proc. Interspeech*, 2019, pp. 1013–1017.

[32] Y. Zhang, W. Wang, and P. Zhang, "The Effect of Silence and Dual-Band Fusion in Anti-Spoofing System," in *Proc. Interspeech 2021*, 2021, pp. 4279–4283.

[33] H. Tak, J. Patino, M. Todisco, A. Nautsch, N. Evans, and A. Larcher, "End-to-End anti-spoofing with RawNet2," in *ICASSP*, 2021, pp. 6369–6373.

[34] H. Tak, J. weon Jung, J. Patino, M. Todisco, and N. Evans, "Graph Attention Networks for Anti-Spoofing," in *Proc. Interspeech*, 2021, pp. 2356–2360.

[35] J. Jung, H. Heo, H. Tak, H. Shim, J. Chung, B. Lee, H. Yu, and N. Evans, "AASIST: Audio anti-spoofing using integrated spectro-temporal graph attention networks," in *2022 IEEE International Conference on Acoustics, Speech, and Signal Processing, ICASSP 2022 - Proceedings*, 2022, pp. 2405–2409.

[36] W. Ge, M. Panariello, J. Patino, M. Todisco, and N. Evans, "Partially-Connected Differentiable Architecture Search for Deepfake and Spoofing Detection," in *Proc. Interspeech*, 2021, pp. 4319–4323.

[37] X. Liu, M. Liu, L. Wang, K. A. Lee, H. Zhang, and J. Dang, "Leveraging positional-related local-global dependency for synthetic speech detection," in *ICASSP*, 2023, pp. 1–5.

[38] R. Prenger, R. Valle, and B. Catanzaro, "Waveglow: A flow-based generative network for speech synthesis," in *ICASSP*, 2019, pp. 3617–3621.

[39] R. Huang, M. W. Lam, J. Wang, D. Su, D. Yu, Y. Ren, and Z. Zhao, "FastDiff: A Fast Conditional Diffusion Model for High-Quality Speech Synthesis," in *Proceedings of the Thirty-First International Joint Conferences on Artificial Intelligence. IJCAI*, 2022.

[40] X. Wang and J. Yamagishi, "Neural Harmonic-plus-Noise Waveform Model with Trainable Maximum Voice Frequency for Text-to-Speech Synthesis," in *10th ISCA Workshop on Speech Synthesis (SSW 10)*, 2019, pp. 1–6.

[41] A. Stan, D. Combei, D. Oneata, and H. Cucu, "TADA: Training-free Attribution and Out-of-Domain Detection of Audio Deepfakes," in *Interspeech 2025*, 2025, pp. 1543–1547.

[42] C.-y. Huang, Y. Y. Lin, H.-y. Lee, and L.-s. Lee, "Defending Your Voice: Adversarial Attack on Voice Conversion," in *2021 IEEE Spoken Language Technology Workshop (SLT)*, 2021, pp. 552–559.

[43] Z. Liu, Y. Zhang, and C. Miao, "Protecting Your Voice from Speech Synthesis Attacks," in *Proceedings of the 39th Annual Computer Security Applications Conference*, ser. ACSAC '23. New York, NY, USA: Association for Computing Machinery, 2023, p. 394–408.

[44] N. Yu, V. Skripniuk, S. Abdelnabi, and M. Fritz, "Artificial Fingerprinting for Generative Models: Rooting Deepfake Attribution in Training Data," in *Proceedings of the IEEE/CVF International Conference on Computer Vision (ICCV)*, October 2021, pp. 14448–14457.

[45] J. Fei, Z. Xia, B. Tondi, and M. Barni, "Robust Retraining-free GAN Fingerprinting via Personalized Normalization," in *2023 IEEE International Workshop on Information Forensics and Security (WIFS)*, 2023, pp. 1–6.

[46] N. Yu, L. Davis, and M. Fritz, "Attributing Fake Images to GANs: Learning and Analyzing GAN Fingerprints," in *Proceedings of the IEEE/CVF International Conference on Computer Vision (ICCV)*, 2019, pp. 7555–7565.

[47] C. Zhang, J. Yi, J. Tao, C. Wang, and X. Yan, "Distinguishing Neural Speech Synthesis Models Through Fingerprints in Speech Waveforms," in *Proceedings of the 23rd Chinese National Conference on Computational Linguistics (Volume 1: Main Conference)*, S. Maosong, L. Jiye, H. Xianpei, L. Zhiyuan, and H. Yulan, Eds. Taiyuan, China: Chinese Information Processing Society of China, Jul. 2024, pp. 1160–1171.

[48] J. Ke and L. Wang, "Understanding and leveraging vocoder fingerprints for synthetic speech attribution," *Applied Intelligence*, vol. 55, p. 673, 2025.

[49] J. Lu, Y. Zhang, Z. Li, Z. Shang, W. Wang, and P. Zhang, "Detecting unknown speech spoofing algorithms with nearest neighbors," in *DADA@IJCAI*, 2023.

[50] X. Qin, X. Wang, Y. Chen, Q. Meng, and M. Li, "From speaker verification to deepfake algorithm recognition: Our learned lessons from ADD2023 track 3," in *DADA@IJCAI*, 2023.

[51] F. Marra, D. Gragnaniello, L. Verdoliva, and G. Poggi, "Do GANs leave artificial fingerprints?" in *2019 IEEE conference on multimedia information processing and retrieval (MIPR)*. IEEE, 2019, pp. 506–511.

[52] A. Défosséz, J. Copet, G. Synnaeve, and Y. Adi, "High Fidelity Neural Audio Compression," *Transactions on Machine Learning Research*, 2023.

[53] A. Podolskiy, D. Lipin, A. Bout, E. Artemova, and I. Piontkovskaya, "Revisiting mahalanobis distance for transformer-based out-of-domain detection," *Proceedings of the AAAI Conference on Artificial Intelligence*, vol. 35, no. 15, pp. 13 675–13 682, May 2021.

[54] F. Behrendt, D. Bhattacharya, R. Mieling, L. Maack, J. Krüger, R. Opfer, and A. Schlaefer, "Leveraging the mahalanobis distance to enhance unsupervised brain MRI anomaly detection," in *Medical Image Computing and Computer Assisted Intervention – MICCAI 2024: 27th International Conference, Marrakesh, Morocco, October 6–10, 2024, Proceedings, Part XI*. Berlin, Heidelberg: Springer-Verlag, 2024, p. 394–404.

[55] K. Ito and L. Johnson, "The LJ Speech Dataset," <https://keithito.com/LJ-Speech-Dataset/>.

[56] K. Gasenzer and M. Wolter, "Towards generalizing deep-audio fake detection networks," *Transactions on Machine Learning Research*, 2024.

[57] K. Kumar, R. Kumar, T. de Boissiere, L. Gestin, W. Z. Teoh, J. Sotelo, A. de Brébisson, Y. Bengio, and A. C. Courville, "Melgan: Generative adversarial networks for conditional waveform synthesis," in *Advances in Neural Information Processing Systems*, H. Wallach, H. Larochelle, A. Beygelzimer, F. d'Alché-Buc, E. Fox, and R. Garnett, Eds., vol. 32. Curran Associates, Inc., 2019.

[58] R. Yamamoto, E. Song, and J.-M. Kim, "Parallel wavegan: A fast waveform generation model based on generative adversarial networks with multi-resolution spectrogram," in *ICASSP 2020 - 2020 IEEE International Conference on Acoustics, Speech and Signal Processing (ICASSP)*, 2020, pp. 6199–6203.

[59] G. Yang, S. Yang, K. Liu, P. Fang, W. Chen, and L. Xie, "Multi-band MelGAN: Faster waveform generation for high-quality text-to-speech," in *Proceedings of the IEEE Spoken Language Technology Workshop (SLT)*, 2021.

[60] J. Kong, J. Kim, and J. Bae, "HiFi-GAN: Generative adversarial networks for efficient and high fidelity speech synthesis," in *Advances in Neural Information Processing Systems*, H. Larochelle, M. Ranzato, R. Hadsell, M. Balcan, and H. Lin, Eds., vol. 33. Curran Associates, Inc., 2020, pp. 17 022–17 033.

[61] T. Bak, J. Lee, H. Bae, J. Yang, J.-S. Bae, and Y.-S. Joo, "Avocodo: generative adversarial network for artifact-free vocoder," in *Proceedings of the Thirty-Seventh AAAI Conference on Artificial Intelligence and Thirty-Fifth Conference on Innovative Applications of Artificial Intelligence and Thirteenth Symposium on Educational Advances in Artificial Intelligence*, ser. AAAI'23/IAAI'23/EAII'23. AAAI Press, 2023.

[62] S.-G. Lee, W. Ping, B. Ginsburg, B. Catanzaro, and S. Yoon, "BigV-GAN: A universal neural vocoder with large-scale training," in *The Eleventh International Conference on Learning Representations*, 2023.

[63] R. Huang, Z. Zhao, H. Liu, J. Liu, C. Cui, and Y. Ren, "ProDiff: Progressive fast diffusion model for high-quality text-to-speech," in *Proceedings of the 30th ACM International Conference on Multimedia*, 2022.

[64] R. Sonobe, S. Takamichi, and H. Saruwatari, "JSUT corpus: free large-scale Japanese speech corpus for end-to-end speech synthesis," *CoRR*, vol. abs/1711.00354, 2017.

[65] X. Wang, J. Yamagishi, M. Todisco, H. Delgado, A. Nautsch, N. Evans, M. Sahidullah, V. Vestman, T. Kinnunen, K. A. Lee, L. Juvela, P. Alku, Y.-H. Peng, H.-T. Hwang, Y. Tsao, H.-M. Wang, S. L. Maguer, M. Becker, F. Henderson, R. Clark, Y. Zhang, Q. Wang, Y. Jia, K. Onuma, K. Mushika, T. Kaneda, Y. Jiang, L.-J. Liu, Y.-C. Wu, W.-C. Huang, T. Toda, K. Tanaka, H. Kameoka, I. Steiner, D. Matrouf, J.-F. Bonastre, A. Govender, S. Ronanki, J.-X. Zhang, and Z.-H. Ling, "ASVspoof 2019: A large-scale public database of synthesized, converted and replayed speech," *Computer Speech & Language*, vol. 64, p. 101114, 2020.

[66] C. Veaux, J. Yamagishi, and K. MacDonald, "CSTR VCTK Corpus: English Multi-speaker Corpus for CSTR Voice Cloning Toolkit [sound]," 2017.

[67] Y. Shi, H. Bu, X. Xu, S. Zhang, and M. Li, "Aishell-3: A multi-speaker mandarin tts corpus," in *Interspeech 2021*, 2021, pp. 2756–2760.

[68] T. Ko, V. Peddinti, D. Povey, M. L. Seltzer, and S. Khudanpur, "A study on data augmentation of reverberant speech for robust speech recognition," in *2017 IEEE International Conference on Acoustics, Speech and Signal Processing (ICASSP)*, 2017, pp. 5220–5224.

[69] M. Pizarro, D. Kolossa, and A. Fisher, "DistriBlock: Identifying adversarial audio samples by leveraging characteristics of the output distribution," in *Proceedings of the Fortieth Conference on Uncertainty in Artificial Intelligence*, ser. Proceedings of Machine Learning Research, N. Kiyavash and J. M. Mooij, Eds., vol. 244. PMLR, 15–19 Jul 2024, pp. 2956–2988.

[70] D. Snyder, D. Garcia-Romero, G. Sell, D. Povey, and S. Khudanpur, "X-Vectors: Robust DNN Embeddings for Speaker Recognition," in *2018 IEEE International Conference on Acoustics, Speech and Signal Processing (ICASSP)*, 2018, pp. 5329–5333.

[71] G. Lavrentyeva, S. Novoselov, A. Tseren, M. Volkova, A. Gorlanov, and A. Kozlov, "STC Antispoofing Systems for the ASVspoof2019 Challenge," in *Interspeech 2019*, 2019, pp. 1033–1037.

[72] K. He, X. Zhang, S. Ren, and J. Sun, "Deep residual learning for image recognition," in *2016 IEEE Conference on Computer Vision and Pattern Recognition (CVPR)*, 2016, pp. 770–778.

[73] J. Hu, L. Shen, and G. Sun, "Squeeze-and-excitation networks," in *2018 IEEE/CVF Conference on Computer Vision and Pattern Recognition*, 2018, pp. 7132–7141.

[74] A. Waibel, T. Hanazawa, G. Hinton, K. Shikano, and K. Lang, "Phoneme recognition using time-delay neural networks," *IEEE Transactions on Acoustics, Speech, and Signal Processing*, vol. 37, no. 3, pp. 328–339, 1989.

[75] V. Peddinti, D. Povey, and S. Khudanpur, "A time delay neural network architecture for efficient modeling of long temporal contexts," in *Interspeech 2015*, 2015, pp. 3214–3218.

[76] X. Wu, R. He, Z. Sun, and T. Tan, "A Light CNN for Deep Face Representation With Noisy Labels," *IEEE Transactions on Information Forensics and Security*, vol. 13, no. 11, pp. 2884–2896, 2018.

[77] P. Khosla, P. Teterwak, C. Wang, A. Sarna, Y. Tian, P. Isola, A. Maschinot, C. Liu, and D. Krishnan, "Supervised Contrastive Learning," in *Advances in Neural Information Processing Systems*, H. Larochelle, M. Ranzato, R. Hadsell, M. Balcan, and H. Lin, Eds., vol. 33. Curran Associates, Inc., 2020, pp. 18 661–18 673.

[78] R. Cipolla, Y. Gal, and A. Kendall, “Multi-task Learning Using Uncertainty to Weigh Losses for Scene Geometry and Semantics,” in *2018 IEEE/CVF Conference on Computer Vision and Pattern Recognition*, 2018, pp. 7482–7491.

IX. APPENDIX

A. Spectral Filter Attribution Comparison

We compare correlation and Mahalanobis single-model attribution in an open world setting to identify the best-performing method for each spectral filter configuration. All residual features are derived from STFT-based acoustic representations with a window size of 8 ms and a hop size of 0.125 ms. This analysis is performed on the ASVspoof 2019 LA benchmark. We set aside two synthesis systems—A16 and A19, which correspond to A04 and A06 in the training set—and construct fingerprints from their samples.

1) *Low-pass filter setup*: This filter method retains only the low-frequency content below the cutoff, potentially emphasizing system-specific spectral characteristics in the lower bands. We evaluate the filters using cutoff frequencies of 1, 3, and 5 kHz.

Results: Based on Table XIII, a 1 kHz cutoff yields the best overall performance, achieving the highest average AUROC when paired with Mahalanobis distance (0.96 for A16 and 1.00 for A19). This configuration slightly outperforms the 3 kHz and 5 kHz cutoffs, making it the preferred setting for low-pass filtering-based residuals.

TABLE XIII

SINGLE-MODEL ATTRIBUTION AUROC SCORES IN AN OPEN-WORLD SETTING USING LOW-PASS FILTER RESIDUALS ON ASVspoof LA. ROWS: SOURCES; COLUMNS: TARGETS. CELLS: CORRELATION / MAHALANOBIS SCORES. HIGHER AUROC VALUES = BETTER SEPARATION BETWEEN THE TARGET SYSTEM AND ALL OTHER SOURCES.

Source\Target	Cutoff = 1 kHz		Cutoff = 3 kHz		Cutoff = 5 kHz	
	A16	A19*	A16	A19*	A16	A19*
A07	0.67 / 0.82	0.97 / 0.99	0.67 / 0.81	0.97 / 0.99	0.63 / 0.78	0.93 / 0.99
A08	0.97 / 1.00	1.00 / 1.00	0.97 / 1.00	1.00 / 1.00	0.95 / 1.00	1.00 / 1.00
A09	0.99 / 1.00	1.00 / 1.00	0.99 / 1.00	1.00 / 1.00	0.99 / 1.00	1.00 / 1.00
A10	0.94 / 1.00	1.00 / 1.00	0.96 / 1.00	1.00 / 1.00	0.96 / 1.00	1.00 / 1.00
A11	0.93 / 1.00	1.00 / 1.00	0.95 / 1.00	1.00 / 1.00	0.96 / 1.00	1.00 / 1.00
A12	0.95 / 1.00	1.00 / 1.00	0.97 / 1.00	1.00 / 1.00	0.98 / 1.00	1.00 / 1.00
A13 [‡]	0.99 / 1.00	1.00 / 1.00	0.99 / 1.00	1.00 / 1.00	0.99 / 1.00	1.00 / 1.00
A14 [‡]	0.98 / 1.00	1.00 / 1.00	0.99 / 1.00	1.00 / 1.00	0.99 / 1.00	1.00 / 1.00
A15 [‡]	0.97 / 1.00	1.00 / 1.00	0.99 / 1.00	1.00 / 1.00	0.98 / 1.00	1.00 / 1.00
A16	-	0.90 / 0.97	-	0.91 / 0.98	-	0.87 / 0.98
A17*	0.89 / 1.00	1.00 / 1.00	0.93 / 1.00	1.00 / 1.00	0.96 / 1.00	1.00 / 1.00
A18*	0.48 / 0.99	0.86 / 0.98	0.57 / 0.99	0.89 / 0.97	0.71 / 0.99	0.91 / 0.99
A19*	0.18 / 0.66	-	0.17 / 0.67	-	0.25 / 0.67	-
Bonafide	0.85 / 1.00	0.99 / 1.00	0.89 / 1.00	1.00 / 1.00	0.93 / 1.00	1.00 / 1.00
Avg.	0.84 / 0.96	0.98 / 1.00	0.86 / 0.95	0.98 / 0.99	0.87 / 0.95	0.97 / 0.99

* VC systems; [‡] TTS+VC; unmarked: TTS only.

2) *High-pass filter setup*: This filter isolates higher-frequency content, which may carry artifacts from synthesis systems. We evaluate the filters using cutoff frequencies of 1, 3, and 5 kHz.

Results: While Mahalanobis distance consistently outperforms correlation as reported in Table XIV, the overall attribution performance of high-pass filtered residuals is notably lower than that of low-pass filtering (see Table XIII).

3) *Band-stop filter setup*: This filter removes mid-to-high-frequency ranges, useful for testing whether the removed band contains synthesis-specific features. We evaluate the filters with stop bands of 4–7 kHz and 5–6 kHz.

TABLE XIV
SINGLE-MODEL ATTRIBUTION AUROC SCORES IN AN OPEN-WORLD SETTING USING HIGH-PASS FILTER RESIDUALS ON ASVspoof LA. ROWS: SOURCES; COLUMNS: TARGETS. CELLS: CORRELATION / MAHALANOBIS SCORES. HIGHER AUROC VALUES = BETTER SEPARATION BETWEEN THE TARGET SYSTEM AND ALL OTHER SOURCES.

Source\Target	Cutoff = 1 kHz		Cutoff = 3 kHz		Cutoff = 5 kHz	
	A16	A19*	A16	A19*	A16	A19*
A07	0.69 / 0.68	0.96 / 0.98	0.70 / 0.71	0.83 / 0.97	0.75 / 0.75	0.86 / 0.97
A08	0.70 / 0.97	0.96 / 1.00	0.92 / 0.97	0.97 / 1.00	0.92 / 0.99	0.92 / 1.00
A09	0.91 / 0.95	0.99 / 1.00	0.85 / 0.94	0.95 / 1.00	0.70 / 0.97	0.79 / 1.00
A10	0.63 / 0.87	0.94 / 1.00	0.72 / 0.93	0.85 / 0.99	0.72 / 0.96	0.85 / 1.00
A11	0.66 / 0.84	0.95 / 1.00	0.74 / 0.94	0.85 / 1.00	0.74 / 0.97	0.86 / 1.00
A12	0.60 / 0.82	0.88 / 1.00	0.63 / 0.89	0.76 / 1.00	0.53 / 0.96	0.71 / 1.00
A13 [‡]	0.76 / 0.90	0.98 / 1.00	0.80 / 0.96	0.91 / 1.00	0.80 / 0.98	0.89 / 1.00
A14 [‡]	0.78 / 0.86	0.98 / 1.00	0.81 / 0.96	0.92 / 1.00	0.73 / 0.98	0.82 / 1.00
A15 [‡]	0.62 / 0.79	0.96 / 1.00	0.58 / 0.87	0.78 / 0.99	0.53 / 0.95	0.64 / 0.99
A16	-	0.79 / 0.98	-	0.70 / 0.98	-	0.64 / 0.97
A17*	0.35 / 0.80	0.70 / 0.96	0.39 / 0.85	0.46 / 0.94	0.41 / 0.94	0.46 / 0.97
A18*	0.53 / 0.59	0.47 / 0.88	0.41 / 0.68	0.48 / 0.89	0.36 / 0.78	0.50 / 0.95
A19*	0.60 / 0.55	-	0.42 / 0.52	-	0.43 / 0.60	-
Bonafide	0.49 / 0.77	0.53 / 0.95	0.57 / 0.85	0.66 / 0.95	0.61 / 0.93	0.64 / 0.97
Avg.	0.67 / 0.81	0.84 / 0.98	0.66 / 0.85	0.78 / 0.98	0.63 / 0.91	0.73 / 0.98

* VC systems; [‡] TTS+VC; unmarked: TTS only.

Results: As reported in Table XV, the best average AUROC is achieved with the wider 4–7 kHz stop band using Mahalanobis distance (0.90 for A16 and 0.98 for A19), but this still falls short compared to the low-pass configuration with a 1 kHz cutoff, which reached 0.96 and 1.00, respectively.

TABLE XV
SINGLE-MODEL ATTRIBUTION AUROC SCORES IN AN OPEN-WORLD SETTING USING BAND-STOP FILTER RESIDUALS ON ASVspoof LA. ROWS: SOURCES; COLUMNS: TARGETS. CELLS: CORRELATION / MAHALANOBIS SCORES. HIGHER AUROC VALUES = BETTER SEPARATION BETWEEN THE TARGET SYSTEM AND ALL OTHER SOURCES.

Source\Target	Stop band = 4–7 kHz		Stop band = 5–6 kHz	
	A16	A19*	A16	A19*
A07	0.59 / 0.74	0.82 / 0.97	0.52 / 0.67	0.67 / 0.95
A08	0.77 / 0.99	0.96 / 1.00	0.80 / 0.98	0.91 / 1.00
A09	0.70 / 0.97	0.93 / 1.00	0.44 / 0.94	0.73 / 1.00
A10	0.60 / 0.92	0.82 / 1.00	0.49 / 0.88	0.66 / 0.99
A11	0.61 / 0.96	0.84 / 1.00	0.61 / 0.91	0.77 / 1.00
A12	0.51 / 0.95	0.82 / 1.00	0.46 / 0.93	0.75 / 1.00
A13 [‡]	0.68 / 0.97	0.88 / 1.00	0.57 / 0.95	0.71 / 1.00
A14 [‡]	0.61 / 0.96	0.88 / 1.00	0.43 / 0.92	0.70 / 1.00
A15 [‡]	0.50 / 0.95	0.81 / 1.00	0.46 / 0.91	0.64 / 1.00
A16	-	0.80 / 0.97	-	0.72 / 0.96
A17*	0.37 / 0.96	0.54 / 0.99	0.51 / 0.92	0.54 / 0.99
A18*	0.49 / 0.79	0.48 / 0.83	0.38 / 0.61	0.36 / 0.71
A19*	0.38 / 0.59	-	0.57 / 0.51	-
Bonafide	0.38 / 0.95	0.61 / 0.99	0.51 / 0.89	0.54 / 0.98
Avg.	0.55 / 0.90	0.79 / 0.98	0.50 / 0.85	0.68 / 0.97

* VC systems; [‡] TTS+VC; unmarked: TTS only.

4) *Band-pass filter*: In contrast to band-stop, these preserve only the selected frequency band, allowing analysis of synthesis artifacts isolated to mid-high ranges. We evaluate band-pass filters with pass bands of 4–7 kHz and 5–6 kHz.

Results: Based on Table XVI, these results are on par with those obtained using low-pass filtered residuals, demonstrating that attribution signals are also strongly expressed within these mid-frequency bands.

Based on the spectral filter results, the chosen configurations are the 1 kHz low-pass filter and the 5–6 kHz band-pass filter, both of which demonstrate strong performance. In the main text, the best-performing configuration is used for further analysis.

TABLE XVI

SINGLE-MODEL ATTRIBUTION AUROC SCORES IN AN OPEN-WORLD SETTING USING BAND-PASS FILTER RESIDUALS ON ASVspoof LA. ROWS: SOURCES; COLUMNS: TARGETS. CELLS: CORRELATION / MAHALANOBIS SCORES. HIGHER AUROC VALUES = BETTER SEPARATION BETWEEN THE TARGET SYSTEM AND ALL OTHER SOURCES.

Source\Target	Pass band = 4–7 kHz		Pass band = 5–6 kHz	
	A16	A19*	A16	A19*
A07	0.64 / 0.78	0.89 / 0.98	0.62 / 0.76	0.89 / 0.98
A08	0.90 / 1.00	0.98 / 1.00	0.91 / 1.00	0.99 / 1.00
A09	0.98 / 1.00	1.00 / 1.00	0.97 / 1.00	1.00 / 1.00
A10	0.97 / 1.00	0.99 / 1.00	0.95 / 1.00	0.99 / 1.00
A11	0.97 / 1.00	0.99 / 1.00	0.94 / 1.00	0.98 / 1.00
A12	0.99 / 1.00	1.00 / 1.00	0.97 / 1.00	0.99 / 1.00
A13 [‡]	1.00 / 1.00	1.00 / 1.00	0.99 / 1.00	1.00 / 1.00
A14 [‡]	1.00 / 1.00	1.00 / 1.00	0.99 / 1.00	1.00 / 1.00
A15 [‡]	0.99 / 1.00	0.99 / 1.00	0.98 / 1.00	1.00 / 1.00
A16	-	0.84 / 0.98	-	0.83 / 0.98
A17*	0.98 / 1.00	0.99 / 1.00	0.95 / 1.00	0.98 / 1.00
A18*	0.88 / 1.00	0.92 / 0.99	0.80 / 1.00	0.86 / 0.98
A19*	0.34 / 0.64	-	0.35 / 0.64	-
Bonafide	0.96 / 1.00	0.99 / 1.00	0.92 / 1.00	0.98 / 1.00
Avg.	0.88 / 0.95	0.97 / 1.00	0.88 / 0.97	0.97 / 0.99

* VC systems; [‡] TTS+VC; unmarked: TTS only.

B. Additional Results on STFT Settings

Detailed pairwise AUROC results are reported for the 25 ms window size / 10 ms hop length STFT configuration introduced in Section VI-B. Table XVII provides results on the Augmented LJSpeech benchmark, Table XIX reports the JSUT benchmark, Table XXI covers ASVspoof LA, and Table XXIII shows CodecFake. In addition, full matrices for the adopted 8 ms / 0.125 ms setting are provided in Table XVIII (Augmented LJSpeech benchmark) and Table XX (JSUT benchmark). While Table II in the main text summarizes average AUROC scores across benchmarks, these tables highlight the detailed source-to-target attribution performance.

C. Additional Results: EnCodec-Based Attribution

Detailed pairwise attribution performance using EnCodec-based residuals for single-model attribution in an open-world setting is shown in Tables XXII–XXVI.

Table XXII shows results for the Augmented LJSpeech Benchmark. Table XXIV presents results on the JSUT benchmark. Table XXV summarizes results on the ASVspoof 2019 LA benchmark. Table XXVI shows performance on the CodecFake benchmark, where residual discriminability is reduced for systems generated with EnCodec. Higher AUROC values indicate better separation between the target system and all other sources. For comparison with spectral filtering approaches, see Table V in the main text.

D. Baseline Model Architectures

We describe the network architectures, preprocessing methods, and relevant training details for reproducibility and clarity.

1) *X-vector*: We adopt a time-delay neural network (TDNN)-based X-vector model [74], [75], originally introduced by Snyder et al. [70]. The model consists of five TDNN layers with context sizes {5, 3, 2, 1, 1} and dilations {1, 1, 2, 1, 3}, each followed by ReLU activation and dropout

($p = 0.5$). Statistical pooling (mean and standard deviation) is applied over the time dimension to produce a fixed 1,024-dimensional embedding, which is passed through a two-layer multi-layer perceptron (MLP) with 512 units per layer and finally mapped to class logits via a softmax output layer.

2) *LCNN*: We implement a Light Convolutional Neural Network (LCNN) following the design of Lavrentyeva et al. [71], which incorporates the Max-Feature-Map (MFM) activation [76]. The model consists of nine convolutional blocks with interleaved MFM activations and batch normalization. Selected blocks are followed by max-pooling for spatial down-sampling. An adaptive max-pooling layer aggregates spatial features into a fixed-length vector, which is processed by a two-layer MLP with dropout ($p = 0.75$), batch normalization, and MFM activation. A softmax output layer produces class logits.

3) *ResNet*: We implement a ResNet-18 [72] architecture, composed of four residual stages with 2, 2, 2, and 2 blocks respectively. Each block contains two 3×3 convolutions with batch normalization and ReLU, and includes skip connections with optional downsampling. The network begins with a 7×7 convolution (stride 2), followed by batch normalization, ReLU, and max-pooling. After the residual stages, global average pooling generates a fixed-size feature vector, which is passed to a single MLP head for classification.

4) *SE-ResNet*: We extend the ResNet-18 architecture by integrating Squeeze-and-Excitation (SE) blocks [73] into each residual block. Each SE module applies global average pooling followed by a two-layer MLP (with ReLU and sigmoid activations) to compute channel-wise scaling factors. These are used to reweight feature maps before the residual addition. The overall architecture mirrors that of ResNet-18, with downsampling performed via strided convolutions in the first block of each stage. The final global average pooled feature vector is fed into a classification MLP.

5) *VFD-Net*: We implement a ResNet-18-based architecture adapted from Deng et al. [14], modified to accept 16-channel input features. After standard ResNet layers and four residual stages ($\{64, 128, 256, 512\}$ channels), global average pooling produces a 512-dimensional feature vector. Two heads follow: (1) a classification head using a single fully connected layer, and (2) a projection head, which is a two-layer MLP (128 hidden units, 64 output), using ReLU activation and ℓ_2 normalization for contrastive learning. Training uses a multi-task loss combining cross-entropy and supervised contrastive loss [77], with weighting learned via the uncertainty-based method [78].

For all baselines, the same time-frequency representation is applied as inputs, linear frequency cepstral coefficients, which are extracted using 20 filters and 60 coefficients, with an STFT configured for a window length of 25 ms and a hop length of 10 ms. A Hann window function is applied.

E. Multi-model attribution performance across benchmarks

Table XXVII reports Precision and Recall for the closed-world multi-model attribution task, and Table XXVIII presents

TABLE XVII

SINGLE-MODEL ATTRIBUTION AUROC SCORES IN AN OPEN-WORLD SETTING USING THE AUGMENTED LJ SPEECH BENCHMARK WITH THE 25 MS WINDOW SIZE / 10 MS HOP LENGTH STFT CONFIGURATION AND MAHALANOBIS DISTANCE. ROWS: SOURCES; COLUMNS: TARGETS. EACH CELL SHOWS SCORES FOR LOW-PASS 1 KHZ / BAND-PASS 5–6 KHZ FILTERS. SEE ALSO TABLE II FOR AVERAGE RESULTS ACROSS BENCHMARKS.[†]

Source\Target	FastDiff	ProDiff	MG-L	Avo	BVG	HF-G	MB-MG	PWG	WGlow	NSF
FastDiff	-	0.96 / 0.96	1.00 / 1.00	1.00 / 1.00	1.00 / 1.00	1.00 / 1.00	1.00 / 1.00	1.00 / 1.00	1.00 / 1.00	1.00 / 1.00
ProDiff	0.98 / 0.99	-	1.00 / 1.00	1.00 / 1.00	1.00 / 1.00	1.00 / 1.00	1.00 / 1.00	0.99 / 1.00	1.00 / 1.00	1.00 / 1.00
MG-L	1.00 / 1.00	1.00 / 1.00	-	1.00 / 1.00	1.00 / 1.00	1.00 / 1.00	1.00 / 1.00	1.00 / 1.00	1.00 / 1.00	1.00 / 1.00
Avo	1.00 / 1.00	1.00 / 1.00	1.00 / 1.00	-	1.00 / 0.99	1.00 / 1.00	0.98 / 0.97	0.96 / 0.93	0.99 / 0.98	0.97 / 0.96
BVG	1.00 / 1.00	1.00 / 1.00	1.00 / 1.00	1.00 / 0.99	-	1.00 / 1.00	1.00 / 1.00	1.00 / 1.00	1.00 / 1.00	1.00 / 1.00
HF-G	1.00 / 1.00	1.00 / 1.00	1.00 / 1.00	1.00 / 1.00	1.00 / 1.00	-	1.00 / 1.00	1.00 / 1.00	1.00 / 0.99	1.00 / 1.00
MB-MG	1.00 / 1.00	1.00 / 1.00	1.00 / 1.00	0.97 / 0.96	1.00 / 1.00	1.00 / 1.00	-	0.97 / 0.96	1.00 / 1.00	1.00 / 1.00
PWG	1.00 / 1.00	1.00 / 1.00	1.00 / 1.00	0.95 / 0.92	1.00 / 0.99	1.00 / 1.00	0.98 / 0.98	-	0.99 / 0.98	0.94 / 0.93
WGlow	1.00 / 1.00	1.00 / 1.00	1.00 / 1.00	1.00 / 1.00	1.00 / 1.00	1.00 / 0.99	1.00 / 1.00	1.00 / 1.00	-	1.00 / 1.00
NSF	1.00 / 1.00	1.00 / 1.00	1.00 / 1.00	0.98 / 0.97	1.00 / 1.00	1.00 / 1.00	1.00 / 1.00	0.95 / 0.93	1.00 / 0.99	-
Real	1.00 / 1.00	1.00 / 1.00	1.00 / 1.00	0.98 / 0.97	1.00 / 1.00	1.00 / 1.00	0.97 / 0.96	0.98 / 0.97	1.00 / 1.00	1.00 / 1.00
Avg.	1.00 / 1.00	1.00 / 1.00	1.00 / 1.00	0.99 / 0.98	1.00 / 1.00	1.00 / 1.00	0.99 / 0.99	0.98 / 0.98	1.00 / 0.99	0.99 / 0.99

[†] Higher AUROC values = better separation between the target system and all other sources.

TABLE XVIII

SINGLE-MODEL ATTRIBUTION AUROC SCORES IN AN OPEN-WORLD SETTING USING THE AUGMENTED LJ SPEECH BENCHMARK WITH THE 8 MS WINDOW SIZE / 0.125 MS HOP LENGTH STFT CONFIGURATION AND MAHALANOBIS DISTANCE. ROWS: SOURCES; COLUMNS: TARGETS. EACH CELL SHOWS SCORES FOR LOW-PASS 1 KHZ / BAND-PASS 5–6 KHZ FILTERS. SEE ALSO TABLE II FOR AVERAGE RESULTS ACROSS BENCHMARKS.[†]

Source\Target	FastDiff	ProDiff	MG-L	Avo	BVG	HF-G	MB-MG	PWG	WGlow	NSF
FastDiff	-	1.00 / 1.00	1.00 / 1.00	1.00 / 1.00	1.00 / 1.00	1.00 / 1.00	1.00 / 1.00	1.00 / 1.00	1.00 / 1.00	1.00 / 1.00
ProDiff	1.00 / 1.00	-	1.00 / 1.00	1.00 / 1.00	1.00 / 1.00	1.00 / 1.00	1.00 / 1.00	1.00 / 1.00	1.00 / 1.00	1.00 / 1.00
MG-L	1.00 / 1.00	1.00 / 1.00	-	1.00 / 1.00	1.00 / 1.00	1.00 / 1.00	1.00 / 1.00	1.00 / 1.00	1.00 / 1.00	1.00 / 1.00
Avo	1.00 / 1.00	1.00 / 1.00	1.00 / 1.00	-	1.00 / 1.00	1.00 / 1.00	1.00 / 1.00	1.00 / 1.00	1.00 / 1.00	1.00 / 1.00
BVG	1.00 / 1.00	1.00 / 1.00	1.00 / 1.00	1.00 / 1.00	-	1.00 / 1.00	1.00 / 1.00	1.00 / 1.00	1.00 / 1.00	1.00 / 1.00
HF-G	1.00 / 1.00	1.00 / 1.00	1.00 / 1.00	1.00 / 1.00	1.00 / 1.00	-	1.00 / 1.00	1.00 / 1.00	1.00 / 1.00	1.00 / 1.00
MB-MG	1.00 / 1.00	1.00 / 1.00	1.00 / 1.00	1.00 / 1.00	1.00 / 1.00	1.00 / 1.00	-	1.00 / 1.00	1.00 / 1.00	1.00 / 1.00
PWG	1.00 / 1.00	1.00 / 1.00	1.00 / 1.00	0.99 / 0.99	0.99 / 0.99	1.00 / 1.00	1.00 / 1.00	-	1.00 / 1.00	0.99 / 0.99
WGlow	1.00 / 1.00	1.00 / 1.00	1.00 / 1.00	1.00 / 1.00	1.00 / 1.00	1.00 / 1.00	1.00 / 1.00	1.00 / 1.00	-	1.00 / 1.00
NSF	1.00 / 1.00	1.00 / 1.00	1.00 / 1.00	1.00 / 1.00	1.00 / 1.00	1.00 / 1.00	1.00 / 1.00	1.00 / 0.99	1.00 / 1.00	-
Real	1.00 / 1.00	1.00 / 1.00	1.00 / 1.00	1.00 / 1.00	1.00 / 1.00	1.00 / 1.00	1.00 / 1.00	1.00 / 1.00	1.00 / 1.00	1.00 / 1.00
Avg.	1.00 / 1.00	1.00 / 1.00	1.00 / 1.00	1.00 / 1.00	1.00 / 1.00	1.00 / 1.00	1.00 / 1.00	1.00 / 1.00	1.00 / 1.00	1.00 / 1.00

[†] Higher AUROC values = better separation between the target system and all other sources.

TABLE XIX

SINGLE-MODEL ATTRIBUTION AUROC SCORES IN AN OPEN-WORLD SETTING ON JSUT BENCHMARK WITH THE 25 MS WINDOW SIZE / 10 MS HOP LENGTH STFT CONFIGURATION AND MAHALANOBIS DISTANCE. ROWS: SOURCES; COLUMNS: TARGETS. CELLS: SCORES FOR LOW-PASS 1 KHZ / BAND-PASS 5–6 KHZ FILTERS.[†]

Source\Target	MB-MG	PWG
MB-MG	-	1.00 / 1.00
PWG	1.00 / 1.00	-
Real	1.00 / 1.00	1.00 / 1.00
Avg.	1.00 / 1.00	1.00 / 1.00

[†] Higher AUROC values = better separation.

TABLE XX

SINGLE-MODEL ATTRIBUTION AUROC SCORES IN AN OPEN-WORLD SETTING ON JSUT BENCHMARK WITH THE 8 MS WINDOW SIZE / 0.125 MS HOP LENGTH STFT CONFIGURATION AND MAHALANOBIS DISTANCE. ROWS: SOURCES; COLUMNS: TARGETS. CELLS: SCORES FOR LOW-PASS 1 KHZ / BAND-PASS 5–6 KHZ FILTERS.[†]

Source\Target	MB-MG	PWG
MB-MG	-	1.00 / 1.00
PWG	1.00 / 1.00	-
Real	1.00 / 1.00	1.00 / 1.00
Avg.	1.00 / 1.00	1.00 / 1.00

[†] Higher AUROC values = better separation.

TABLE XXI

SINGLE-MODEL ATTRIBUTION AUROC SCORES IN AN OPEN-WORLD SETTING ON ASVspoof LA WITH THE 25 MS WINDOW SIZE / 10 MS HOP LENGTH STFT CONFIGURATION AND MAHALANOBIS DISTANCE. ROWS: SOURCES; COLUMNS: TARGETS. CELLS: SCORES FOR LOW-PASS 1 KHZ / BAND-PASS 5–6 KHZ FILTERS.[†]

Source\Target	A01	A02	A03	A04	A05	A06
A01	-	1.00 / 1.00	1.00 / 1.00	0.80 / 0.76	1.00 / 1.00	1.00 / 1.00
A02	0.94 / 0.98	-	0.44 / 0.87	0.88 / 0.98	0.77 / 0.74	1.00 / 1.00
A03	0.98 / 1.00	0.99 / 1.00	-	0.96 / 0.98	0.91 / 0.95	1.00 / 1.00
A04	0.84 / 0.92	1.00 / 1.00	1.00 / 1.00	-	1.00 / 1.00	0.99 / 1.00
A05	0.97 / 0.98	0.99 / 0.99	0.72 / 0.95	0.88 / 0.98	-	1.00 / 1.00
A06	0.84 / 0.82	1.00 / 1.00	1.00 / 1.00	0.71 / 0.71	1.00 / 1.00	-
A07	0.85 / 0.79	1.00 / 1.00	1.00 / 1.00	0.81 / 0.77	1.00 / 1.00	0.99 / 0.99
A08	1.00 / 1.00	1.00 / 1.00	1.00 / 1.00	1.00 / 1.00	1.00 / 1.00	1.00 / 1.00
A09	0.99 / 1.00	1.00 / 1.00	0.81 / 0.97	0.98 / 0.98	0.90 / 0.99	1.00 / 1.00
A10	0.99 / 0.99	1.00 / 1.00	0.90 / 0.92	0.98 / 0.98	0.95 / 0.95	1.00 / 1.00
A11	1.00 / 1.00	1.00 / 1.00	0.98 / 0.99	0.99 / 0.99	0.99 / 0.99	1.00 / 1.00
A12	1.00 / 1.00	1.00 / 1.00	0.92 / 0.98	0.97 / 0.98	0.95 / 1.00	1.00 / 1.00
A13	1.00 / 1.00	1.00 / 1.00	0.92 / 0.94	0.99 / 0.99	0.96 / 0.97	1.00 / 1.00
A14	0.99 / 0.99	1.00 / 1.00	0.86 / 0.90	0.99 / 0.99	0.94 / 0.95	1.00 / 1.00
A15	1.00 / 1.00	1.00 / 1.00	0.89 / 0.91	0.98 / 0.98	0.90 / 0.91	1.00 / 1.00
A17	0.99 / 0.98	1.00 / 1.00	0.92 / 0.97	0.95 / 0.97	0.88 / 0.91	1.00 / 1.00
A18	0.95 / 0.92	1.00 / 1.00	0.83 / 0.90	0.84 / 0.87	0.91 / 0.94	0.95 / 0.98
Bonafide	0.99 / 0.99	1.00 / 1.00	0.95 / 0.98	0.95 / 0.96	0.95 / 0.95	1.00 / 1.00
Avg.	0.96 / 0.96	1.00 / 1.00	0.89 / 0.96	0.92 / 0.93	0.94 / 0.96	1.00 / 1.00

[†] Higher AUROC values = better separation between the target system and all other sources.

the corresponding standard-deviation values, averaged over 5 independent runs with 10 training epochs per trial. Complementary Accuracy and F1-score results appear in Table XI in the main text.

TABLE XXII

SINGLE-MODEL ATTRIBUTION AUROC SCORES IN AN OPEN-WORLD SETTING USING ENCODEC FILTER ON THE AUGMENTED LJ SPEECH BENCHMARK. ROWS: SOURCES; COLUMNS: TARGETS. CELLS: CORRELATION / MAHALANOBIS SCORES. SEE ALSO TABLE V FOR AVERAGE RESULTS.[†]

Source\Target	FastDiff	ProDiff	MG-L	Avo	BVG	HF-G	MB-MG	PWG	WGlow	NSF
FastDiff	-	1.00 / 0.88	1.00 / 1.00	1.00 / 1.00	1.00 / 1.00	1.00 / 0.98	1.00 / 1.00	1.00 / 0.98	1.00 / 0.99	1.00 / 0.97
ProDiff	0.98 / 0.85	-	1.00 / 1.00	1.00 / 0.99	1.00 / 0.99	1.00 / 0.96	1.00 / 1.00	1.00 / 0.95	1.00 / 0.97	1.00 / 0.94
MG-L	1.00 / 1.00	1.00 / 1.00	-	1.00 / 1.00	1.00 / 1.00	1.00 / 1.00	1.00 / 1.00	1.00 / 1.00	1.00 / 1.00	0.99 / 1.00
Avo	1.00 / 1.00	1.00 / 0.99	1.00 / 0.99	-	0.99 / 0.94	1.00 / 0.95	0.96 / 0.84	0.96 / 0.88	0.99 / 0.88	0.78 / 0.82
BVG	1.00 / 1.00	1.00 / 1.00	1.00 / 1.00	0.97 / 0.95	-	1.00 / 0.98	0.98 / 0.97	0.98 / 0.98	0.98 / 0.97	0.93 / 0.96
HF-G	1.00 / 0.99	1.00 / 0.96	1.00 / 1.00	1.00 / 0.94	1.00 / 0.97	-	1.00 / 0.94	1.00 / 0.94	1.00 / 0.90	0.94 / 0.88
MB-MG	1.00 / 1.00	1.00 / 1.00	1.00 / 0.99	0.91 / 0.80	0.98 / 0.94	1.00 / 0.95	-	0.96 / 0.87	0.99 / 0.92	0.93 / 0.87
PWG	1.00 / 0.99	1.00 / 0.98	1.00 / 1.00	0.98 / 0.84	1.00 / 0.95	0.99 / 0.90	0.99 / 0.86	-	0.98 / 0.86	0.79 / 0.76
WGlow	1.00 / 0.98	1.00 / 0.97	1.00 / 1.00	0.99 / 0.92	1.00 / 0.94	0.98 / 0.89	1.00 / 0.94	0.99 / 0.91	-	0.92 / 0.89
NSF	1.00 / 0.99	1.00 / 0.96	1.00 / 1.00	0.99 / 0.86	1.00 / 0.96	0.98 / 0.85	1.00 / 0.90	0.98 / 0.81	0.99 / 0.85	-
Real	1.00 / 1.00	1.00 / 1.00	1.00 / 1.00	0.97 / 0.91	0.99 / 0.97	1.00 / 0.98	0.95 / 0.90	0.99 / 0.93	1.00 / 0.96	0.96 / 0.92
Avg.	1.00 / 0.98	1.00 / 0.97	1.00 / 1.00	0.98 / 0.92	1.00 / 0.97	0.99 / 0.94	0.99 / 0.93	0.99 / 0.93	0.99 / 0.93	0.92 / 0.90

[†] Higher AUROC values = better separation between the target system and all other sources.

TABLE XXIII

SINGLE-MODEL ATTRIBUTION AUROC SCORES IN AN OPEN-WORLD SETTING ON CODECFAKE WITH THE 25 MS WINDOW SIZE / 10 MS HOP LENGTH STFT CONFIGURATION AND MAHALANOBIS DISTANCE. ROWS: SOURCES; COLUMNS: TARGETS. CELLS: SCORES FOR LOW-PASS 1 KHZ / BAND-PASS 5–6 KHZ FILTERS.[†]

Source\Target	C1	C2	C3	C4	C5	C6
C1	-	1.00 / 1.00	1.00 / 1.00	1.00 / 1.00	1.00 / 1.00	1.00 / 1.00
C2	0.99 / 0.99	-	1.00 / 1.00	0.98 / 0.99	0.99 / 0.99	0.88 / 0.92
C3	1.00 / 1.00	1.00 / 1.00	-	1.00 / 1.00	1.00 / 1.00	1.00 / 1.00
C4	1.00 / 1.00	0.99 / 0.99	1.00 / 1.00	-	1.00 / 1.00	0.99 / 1.00
C5	1.00 / 1.00	0.96 / 0.96	1.00 / 1.00	0.99 / 0.99	-	0.95 / 0.97
C6	0.99 / 0.98	0.84 / 0.83	1.00 / 1.00	0.97 / 0.98	0.97 / 0.97	-
C7	1.00 / 0.99	0.92 / 0.93	1.00 / 1.00	0.98 / 0.99	0.99 / 0.99	0.89 / 0.92
Real	1.00 / 1.00	0.97 / 0.97	1.00 / 1.00	1.00 / 1.00	1.00 / 1.00	0.97 / 0.97
Avg.	1.00 / 0.99	0.96 / 0.96	1.00 / 1.00	0.99 / 0.99	0.99 / 0.99	0.95 / 0.97

[†] Higher AUROC values = better separation between the target system and all other sources.

TABLE XXIV

SINGLE-MODEL ATTRIBUTION AUROC SCORES IN AN OPEN-WORLD SETTING USING ENCODEC FILTER ON THE JSUT BENCHMARK. ROWS: SOURCES; COLUMNS: TARGETS. CELLS: CORRELATION / MAHALANOBIS SCORES.[†]

Source\Target	MB-MG	PWG
MB-MG	-	0.99 / 1.00
PWG	1.00 / 0.99	-
Real	1.00 / 1.00	1.00 / 1.00
Avg.	1.00 / 0.99	1.00 / 1.00

[†] Higher AUROC values = better separation.

TABLE XXV

SINGLE-MODEL ATTRIBUTION AUROC SCORES IN AN OPEN-WORLD SETTING USING ENCODEC FILTER ON THE ASVspoof LA BENCHMARK. ROWS: SOURCES; COLUMNS: TARGETS. CELLS: CORRELATION / MAHALANOBIS SCORES.[†]

Source\Target	A01	A02	A03	A04	A05	A06
A01	-	1.00 / 1.00	1.00 / 0.99	0.81 / 0.69	1.00 / 1.00	0.97 / 0.97
A02	1.00 / 0.80	-	0.86 / 0.83	1.00 / 0.79	0.67 / 0.52	1.00 / 0.99
A03	1.00 / 0.89	0.97 / 0.97	-	1.00 / 0.81	0.99 / 0.88	1.00 / 1.00
A04	0.61 / 0.62	1.00 / 1.00	1.00 / 0.99	-	1.00 / 1.00	0.83 / 0.95
A05	1.00 / 0.80	0.72 / 0.96	0.89 / 0.92	1.00 / 0.79	-	
A06	0.87 / 0.72	1.00 / 1.00	1.00 / 0.99	0.81 / 0.72	1.00 / 0.98	-
A07	0.52 / 0.66	1.00 / 1.00	1.00 / 1.00	0.61 / 0.72	1.00 / 1.00	0.91 / 0.96
A08	0.96 / 0.81	1.00 / 1.00	1.00 / 0.97	0.96 / 0.85	1.00 / 0.99	0.94 / 1.00
A09	1.00 / 0.91	0.99 / 0.99	0.84 / 0.83	1.00 / 0.85	0.99 / 0.92	1.00 / 1.00
A10	1.00 / 0.83	0.99 / 0.97	0.94 / 0.83	1.00 / 0.79	0.99 / 0.80	1.00 / 0.98
A11	1.00 / 0.90	0.99 / 1.00	0.94 / 0.94	1.00 / 0.89	0.99 / 0.93	1.00 / 1.00
A12	1.00 / 0.88	0.99 / 0.99	0.94 / 0.84	1.00 / 0.81	0.99 / 0.87	1.00 / 1.00
A13	1.00 / 0.82	1.00 / 0.97	0.97 / 0.80	1.00 / 0.79	1.00 / 0.75	1.00 / 0.99
A14	1.00 / 0.88	0.99 / 0.98	0.95 / 0.86	1.00 / 0.88	0.99 / 0.85	1.00 / 1.00
A15	1.00 / 0.81	0.95 / 0.96	0.81 / 0.78	1.00 / 0.74	0.95 / 0.73	1.00 / 0.99
A17	1.00 / 0.80	0.90 / 1.00	0.90 / 0.93	1.00 / 0.77	0.79 / 0.73	0.99 / 0.97
A18	1.00 / 0.73	0.98 / 0.98	0.97 / 0.84	1.00 / 0.66	0.97 / 0.64	0.97 / 0.93
Bonafide	1.00 / 0.83	0.92 / 1.00	0.91 / 0.94	1.00 / 0.79	0.89 / 0.84	0.99 / 0.98
Avg.	0.94 / 0.81	0.96 / 0.99	0.94 / 0.90	0.95 / 0.78	0.95 / 0.85	0.98 / 0.98

[†] Higher AUROC values = better separation between the target system and all other sources.

TABLE XXVI

SINGLE-MODEL ATTRIBUTION AUROC SCORES IN AN OPEN-WORLD SETTING USING ENCODEC FILTER ON THE CODECFAKE BENCHMARK. ROWS: SOURCES; COLUMNS: TARGETS. CELLS: CORRELATION / MAHALANOBIS SCORES.[†]

Source\Target	C1	C2	C3	C4	C5	C6
C1	-	0.94 / 0.89	1.00 / 0.99	0.97 / 1.00	0.97 / 0.94	0.92 / 0.89
C2	0.70 / 0.77	-	1.00 / 0.98	0.91 / 1.00	0.78 / 0.84	0.57 / 0.73
C3	1.00 / 0.99	1.00 / 1.00	-	1.00 / 1.00	1.00 / 1.00	1.00 / 0.99
C4	0.68 / 0.48	0.73 / 0.44	1.00 / 0.86	-	0.84 / 0.52	0.64 / 0.39
C5	0.70 / 0.80	0.59 / 0.80	1.00 / 0.98	0.89 / 0.99	-	0.57 / 0.80
C6	0.68 / 0.75	0.64 / 0.73	1.00 / 0.98	0.91 / 0.99	0.82 / 0.82	-
C7	0.72 / 0.81	0.61 / 0.77	1.00 / 0.98	0.91 / 0.99	0.75 / 0.86	0.58 / 0.75
Real	0.88 / 0.91	0.89 / 0.92	1.00 / 0.99	0.97 / 1.00	0.95 / 0.96	0.88 / 0.90
Avg.	0.77 / 0.79	0.77 / 0.79	1.00 / 0.97	0.94 / 1.00	0.87 / 0.85	0.74 / 0.78

[†] Higher AUROC values = better separation between the target system and all other sources.

TABLE XXVII

CLOSED-WORLD MULTI-MODEL ATTRIBUTION PERFORMANCE OF RFP CLASSIFIERS COMPARED TO BASELINES ACROSS BENCHMARKS. CELLS: PRECISION / RECALL, AVG. OVER 5 RUNS WITH 10 EPOCHS EACH.

Model	Augm. LJSpeech	JSUT	ASVspoof	CodecFake
X-vector	0.99 / 0.99	0.99 / 0.99	1.00 / 1.00	1.00 / 1.00
LCNN	0.98 / 0.98	0.98 / 0.98	1.00 / 1.00	0.99 / 0.98
ResNet	0.98 / 0.98	0.99 / 0.99	1.00 / 1.00	1.00 / 1.00
SE-ResNet	0.98 / 0.98	1.00 / 1.00	1.00 / 1.00	1.00 / 1.00
RFP (ours)	1.00 / 1.00	1.00 / 1.00	0.97 / 0.97	0.99 / 0.99
RFP CNN (ours)	1.00 / 1.00	1.00 / 1.00	1.00 / 1.00	1.00 / 1.00
	0.0027 / 0.0027	0.0033 / 0.0033	0.0003 / 0.0003	0.0010 / 0.0010
	0.0092 / 0.0092	0.0157 / 0.0157	0.0011 / 0.0011	0.0028 / 0.0028
	0.0080 / 0.0080	0.0150 / 0.0150	0.0005 / 0.0005	0.0031 / 0.0031
	0.0109 / 0.0113	0.0035 / 0.0035	0.0003 / 0.0003	0.0016 / 0.0016
	0.0001 / 0.0001	0.0000 / 0.0000	0.0010 / 0.0010	0.0010 / 0.0010
	0.0002 / 0.0002	0.0081 / 0.0081	0.0014 / 0.0014	0.0003 / 0.0003

F. Real vs. Synthetic classification performance across benchmarks

Table XXIX reports Precision and Recall for the real vs. synthetic classification task, and Table XXX presents the corresponding standard-deviation values, averaged over 5 independent runs with 10 training epochs per trial. Complementary Accuracy and F1-score results appear in Table XII in the main text.

TABLE XXIX

REAL VS. SYNTHETIC CLASSIFICATION PERFORMANCE OF OUR RFP CNN
 COMPARED TO BASELINES ACROSS BENCHMARKS. CELLS: PRECISION /
 RECALL, AVG. OVER 5 RUNS WITH 10 EPOCHS OF TRAINING EACH.

Model	Augm. LJSpeech	JSUT	ASVspoof	CodecFake
X-vector	0.88 / 0.99	1.00 / 1.00	0.95 / 0.80	1.00 / 0.86
LCNN	0.96 / 0.97	0.98 / 1.00	0.97 / 0.89	0.95 / 0.92
ResNet	0.98 / 0.99	1.00 / 1.00	0.99 / 0.90	1.00 / 0.87
SE-ResNet	0.98 / 0.99	1.00 / 1.00	0.99 / 0.90	1.00 / 0.87
RFP CNN (ours)	1.00 / 1.00	1.00 / 1.00	1.00 / 0.91	1.00 / 0.87

TABLE XXX

REAL VS. SYNTHETIC CLASSIFICATION PERFORMANCE OF OUR RFP CNN
 COMPARED TO BASELINES ACROSS BENCHMARKS. CELLS: STANDARD
 DEVIATION OF ACCURACY / STANDARD DEVIATION OF F1 SCORE, AVG.
 OVER 5 RUNS WITH 10 EPOCHS OF TRAINING EACH.

Model	Augm. LJSpeech	JSUT	ASVspoof	CodecFake
X-vector	0.1367 / 0.0991	0.0000 / 0.0000	0.0333 / 0.0470	0.0022 / 0.0025
LCNN	0.0077 / 0.0073	0.0228 / 0.0216	0.0140 / 0.0156	0.0197 / 0.0179
ResNet	0.0013 / 0.0012	0.0009 / 0.0009	0.0076 / 0.0086	0.0059 / 0.0067
SE-ResNet	0.0046 / 0.0044	0.0000 / 0.0000	0.0073 / 0.0081	0.0070 / 0.0081
RFP CNN (ours)	0.0028 / 0.0028	0.0004 / 0.0004	0.0143 / 0.0158	0.0029 / 0.0033